NASA Technical Memcrandum 100769

Gravity Field Error Analysis: Applications of GPS Receivers and Gradiometers on Low Orbiting Platforms

E. Schrama

November 1990

NASA

NASA Technical Memorandum 100769

Gravity Field Error Analysis: Applications of GPS Receivers and Gradiometers on Low Orbiting Platforms

E. Schrama
Goddard Space Flight Center
Greenbelt, Maryland

National Aeronautics and
Space Administration

Goddard Space Flight Center
Greenbelt, MD

1990

Abstract

The concept of a GPS receiver as a tracking facility and a gradiometer as a separate instrument on a low orbiting platform offers a unique tool to map the Earth's gravitational field with unprecedented accuracies. The former technique allows determination of the spacecraft's ephemeris at any epoch to within 3 to 10 cm, the latter permits the measurement of the tensor of second order derivatives of the gravity field to within 0.01 to 0.0001 Eötvös units depending on the type of gradiometer. The first part of this report describes a variety of error sources in gradiometry where emphasis is placed on the rotational problem pursuing as well a static as a dynamic approach. In the second part, an analytical technique is described and applied for an error analysis of gravity field parameters from gradiometer and GPS observation types. Results are discussed for various configurations proposed on Topex/Poseidon, Gravity Probe-B and Aristoteles, indicating that "GPS only" solutions may be computed up to degree and order 35,55 and 85 respectively, whereas a combined GPS/gradiometer experiment on Aristoteles may result in an acceptable solution up to degree and order 240.

Contents

Chapter 1

Introduction

Before a gravity gradiometer was considered as an instrument on a spacecraft, Wolff (1969) suggested a mission where one satellite tracks another [satellite to satellite tracking or SST] with the intention of measuring the Earth's gravitational field. The low-low version of this idea has been demonstrated in the ATS 6/Apollo-Soyuz mission cf (VonBun et al.,1980), whereas an actual dedicated low-low Gravity Research Mission (GRM), as considered in a proposal of the National Aeronautics and Space Administration (NASA) cf (Keating et al.,1986), was never realized. The high-low version of SST was successfully demonstrated by ATS 6 tracking GEOS-3 cf (Hajela,1978). A similar technique is used for solving lunar and planetary gravity models where velocity perturbations of orbiters are observed on Earth as a Doppler shift in the returned radio signals.

Gradiometry can be considered as a variation of the low-low version of SST realized inside one satellite cf (Rummel,1986). Currently there exists a proposal within the European Space Agency [ESA] to launch a gravity gradiometer satellite called Aristoteles in the time frame of 1996 to 1998. The mission objectives are to measure the Earth's gravity field to within 5 mgal for gravity anomalies and 10 cm for geoid heights with a spacial resolution of 100 km. Aristoteles will be placed in a near circular sun-synchronous orbit [$I = 96.33°$] at a height of 200 km. The spacecraft will carry a 0.01 E/$\sqrt{\text{Hz}}$ 2-axis gradiometer [instrument frame perpendicular to the satellite's velocity vector] and a GPS receiver which should allow instantaneous estimates of the position to within the sub-decimeter noise level.

The concept of GPS as a tracking facility on an orbiting platform has also been suggested for TOPEX/Poseidon [Ocean/Topography Experiment] and GP-B [Gravity probe B, a relativistic experiment]. The advantage of GPS is that continuous accurate tracking is made possible, allowing the estimation of positions and velocities of the spacecraft at each epoch along the orbit. Currently tracking is performed mainly by means of laser and Doppler measurements from ground based stations to satellites implying that the orbit is covered only up to a few percent with actual

measurements.

The technique for analyzing gravity field errors from GPS position estimates and gradiometer observations reported here has been applied in preliminary studies of Aristoteles, cf (ESA,1989) and (Koop et al.,1989). Initially we started with a technique for treating the gradiometer problem developed in (Colombo,1988) and included later the GPS part after ESA decided to consider GPS, instead of PRARE, on Aristoteles. The GPS part in the error analysis is somehow similar to the problem described by Smith et al. (1988) for GP-B. Unfortunately a complete error analysis of Aristoteles was not directly possible with the available techniques since it requires consideration of 1) a non-polar inclination, 2) a limited bandwidth of the gradiometer possibly with a colored noise spectrum and 3) the treatment of the GPS and gradiometer aspect simultaneously.

This was the reason to reformulate the original technique in a "frequency like approach" in which the observation equations are considered for lumped coefficients in the spectral domain. This has been done for both the gradiometer and GPS observation equations thereby avoiding explicit analytical expressions of elements in the normal matrix. Thus any frequency dependent behavior of an instrument may be modeled by means of an a priori covariance function for the noise in the observations.

The organization of Chapters and Appendices in this report is as follows. Chapter 2 treats some principles of gradiometry in view of Aristoteles, the nominal orbit definition, a variety of error sources such as orbital errors, rotational effects including scale, coupling and non-linearity of the gradiometer and the problem of self gravitation. Chapter 3 describes briefly the mathematics behind the error analysis, expressions for observation equations and the derivation of normal equations, followed by a discussion of the results for various cases. Finally Chapter 4 contains conclusions and recommendations for this technique and for gravity field improvement in general. Two Appendices discuss some specific problems encountered, most of them are not directly related to the actual problem.

Acknowledgements

I would like to thank Oscar Colombo [University of Maryland], Reiner Rummel and Radboud Koop [both at the Delft University of Technology, faculty of Geodesy] and Srinivas Bettadpur [Center for Space Research, The University of Texas] for their valuable suggestions and Jeff Ridgway [ST systems corporation, Lanham, Maryland] for helping me with computer simulations. This research is supported financially in the form of a research fellowship by the Royal Netherlands Academy of Arts and Sciences and through NASA grant NAG 5-245. At the moment of writing the author is visiting NASA's Goddard Space Flight Center at Greenbelt in Maryland.

Chapter 2

Gradiometry

In this Chapter we will discuss the principles of gradiometry, the choice of orbits for proposed missions and some error sources inherent to the concept of gradiometry.

2.1 Principles

On the surface of the Earth, the most straightforward method to detect gravitational acceleration is to measure the time needed for a proof-mass [p.m.] to fall from a certain height, or to observe the period of oscillation of a pendulum with a certain length. Both experiments, in some way applied in gravity meters, have been carried out for geodetic and geophysical purposes to investigate the gravity field in most parts of the world, cf (Vaníček and Krakiwsky,1984).

Unfortunately, in an orbiting spacecraft, both the pendulum and the drop test fail since the satellite itself is continuously falling resulting in a gravity-free environment inside the spacecraft. In this case the only effect that can be observed is the remaining non-conservative force primarily caused by atmospheric drag or radiation pressure acting on the spacecraft. A successfully applied technique is to correct continuously the orbit of a spacecraft by means of small thrusters in such a way that a p.m. remains in the center of mass [c.m.]. The resulting orbit is called drag-free and obeys the equations of motion:

$$\ddot{\overline{x}} = \nabla V + \overline{f} \tag{2.1}$$

where $\ddot{\overline{x}}$ represents the acceleration vector [in an inertial coordinate system], V the gravitational potential function and $\overline{f}$ additional conservative forces.

What would happen if one deployed an accelerometer, consisting of the "p.m. under suspension type", at some distance from the c.m. Clearly something would be observed since the p.m. in the accelerometer would tend to behave as an individual orbiting satellite "falling" in another trajectory than the c.m. of the spacecraft. However the suspension mechanism of the accelerometer would continously drive

the p.m. back to some defined local origin of the accelerometer and as a result one would observe some force acting on the p.m. If one ignores rotational effects of the entire spacecraft then this driving force consists of the difference in gravitational acceleration between the c.m. of the spacecraft and the local origin of the accelerometer. Using the same technique, differences in accelerations due to gravity could be observed at any position in the spacecraft relative to the c.m. or differences in acceleration could be observed between two or more arbitrarily placed accelerometers in a spacecraft. When attached to some frame, e.g. four accelerometers on a base plate or eight accelerometers on the corners of a cube, the instrument is called a gradiometer.

The differences in acceleration observed between accelerometers can be translated to second order derivatives of the potential V, ignoring effects due to rotation which will be discussed later on in this Chapter. Essentially this translation is a direct consequence of the equations of motion eq. (2.1). For two accelerometers at the points P and Q we find that:

$$\ddot{\boldsymbol{x}}_i|_P = \left.\frac{\partial V}{\partial \boldsymbol{x}_i}\right|_P \quad \wedge \quad \ddot{\boldsymbol{x}}_i|_Q = \left.\frac{\partial V}{\partial \boldsymbol{x}_i}\right|_Q$$

A Taylor expansion gives:

$$\ddot{\boldsymbol{x}}_i|_Q = \left.\frac{\partial V}{\partial \boldsymbol{x}_i}\right|_P + \left.\frac{\partial^2 V}{\partial \boldsymbol{x}_i \partial \boldsymbol{x}_j}\right|_P \Delta \boldsymbol{x}_j + O(\Delta \boldsymbol{x}_j^2)$$

where $\Delta \boldsymbol{x}_j = \boldsymbol{x}_j|_Q - \boldsymbol{x}_j|_P$. As a result:

$$\frac{\partial^2 V}{\partial \boldsymbol{x}_i \partial \boldsymbol{x}_j} = \frac{\ddot{\boldsymbol{x}}_i|_Q - \ddot{\boldsymbol{x}}_i|_P}{\Delta \boldsymbol{x}_j} + O(\Delta \boldsymbol{x}_j^2)$$

In total one could observe a tensor of 9 elements of the second order derivatives of V of which 5 components are independent due to symmetry of the tensor and the Laplace condition for the gravitational potential, cf (Rummel,1986).

While the dimension of acceleration is given in m/s^2, second order derivatives are represented in units of $1/s^2$ since differences in accelerations are divided by meters. It is customary to work with so-called Eötvös units [E] which have the dimension of $10^{-9}/s^2$. State-of-art gradiometers can operate at room temperatures with an accuracy of 0.01 E/$\sqrt{\text{Hz}}$ cf (Benz et al., 1988). Gradiometers cooled at super conducting temperatures of a few degrees Kelvin operate with accuracies of 0.0001 E/$\sqrt{\text{Hz}}$ as is described in (Morgan and Paik,1988).

2.2 Orbit selection

2.2.1 Orbital height

Although gradiometers of high accuracies can be built with the present state of technology, there is a need for circular orbits at very low altitudes [160 to 200 km]. A spherical harmonic expansion describing the gravity field shows a natural damping behavior containing a term $(a_e/r)^{l+1}$ for the potential function where a_e represents the mean equatorial radius and r the radial distance between the instrument and the center of mass of the Earth and l the spherical harmonic degree cf (Heiskanen and Moritz, 1967).

Several error analysis studies, more or less similar to the method applied in this report, indicate that gravity fields up to degree and orders around 300 to 500 can be estimated from gradiometers with accuracies ranging from 10^{-2} to 10^{-4} E/$\sqrt{\text{Hz}}$ in orbits ranging from 160 to 200 km. [A summary of these studies can be found in Appendix C of (Morgan & Paik, 1988)]. In most error analysis studies the threshold for recovery in terms of degree and orders is usually determined by comparing the estimated error [here r.m.s.] per coefficient per degree to some a priori assumed signal behavior of the Earth's gravity field such as Kaula's rule of thumb, cf (Kaula,1966b).

2.2.2 Orbital decay

At a height of 200 km an orbit decays about 7 km per day due to atmospheric drag which depends on the intensity of solar radiation and the condition of the Earth's magnetic field. This is shown in figure 2.1 where the height of Aristoteles is displayed as a function of time over a 1 day period. The underlying simulation, cf (Ridgway,1990), involved an integration of the equations of motion using the GEM-T2 gravitational model, cf (Marsh et al., 1986,1989), and the Jacchia 71 model using Cd=3.0, a cross sectional area of 2.3 m^2, mass=1240 kg, Kp=2.2 and F10.7=120 (average=137) 10^{-22} $W/m^2/Hz$. These parameters are chosen according to the specifications of Aristoteles as given in (ESA,1989).

The heights shown in figure 2.1 are with respect to a mean equatorial radius of 6378137 m and show oscillations of the order of 10 km due to a small eccentricity and C_{20} short periodic effects. The dashed line in this figure is the result of fitting a first degree polynomial through the height curve, indicating a slope of -6.8 km per day. For the Aristoteles mission it is foreseen to correct the orbit frequently to prevent a mean height below 190 km which, according to the simulation described above, could occur within 2 days when starting at a mean height of 200 km.

2.2.3 Sun synchronous orbits

Benz et al. (1988) explain the need of a sun synchronous orbit at 200 km height for Aristoteles. This constrains the inclination of the orbit to 96.33° which can be

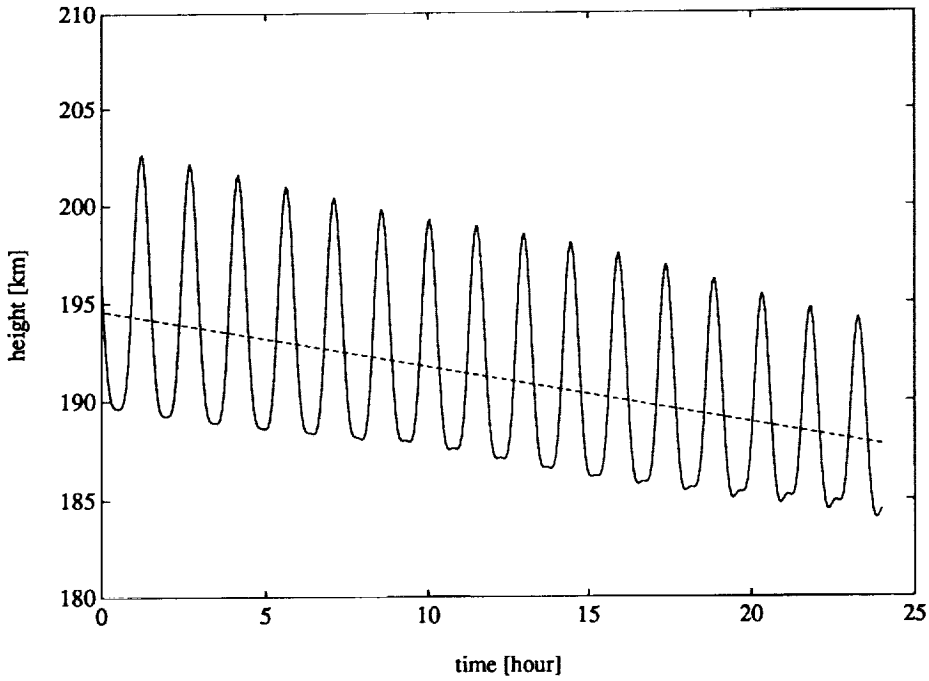

Figure 2.1: Height as a function of time for a simulated Aristoteles arc over a 1 day period. The dashed line is the result of fitting a first degree polynomial through the height curve, indicating a slope of -6.8 km per day.

confirmed by computing the secular motion of Ω due to the flattening term C_{20} [=-0.00108263] of the gravity field:

$$\frac{d\Omega}{dt} = \frac{3nC_{20}a_e^2}{2(1-e^2)^2a^2}\cos I \tag{2.2}$$

where $n = \sqrt{\mu/a^3}$ as is shown by Kaula (1966a). One finds that $2\pi/\dot{\Omega}$ equals to one year, i.e. the rate of Ω is such that the orbital plane rotates about the z-axis of the Earth as fast as the Earth revolves around the sun. Thus it appears for an observer in the satellite that the sun is always in the same position with respect to the orbital plane. Furthermore, in the case of Aristoteles, Ω is chosen such that the sun line is perpendicular to the orbital plane, resulting in a so-called dawn-dusk trajectory.

Despite this geometry, the observer will also notice some yearly variations in the position of the sun due to obliqueness of the Earth's rotational axis with respect to the ecliptic. Nevertheless sun synchronous orbits provide an efficient means of power production by means of solar arrays and a minimal effect of thermal and mechanical noise due to occultation. Figure 4.2 on page 67 in (Morgan & Paik, 1988) clarifies the gravity gradiometer orbital lighting geometry in a sun synchronous orbit.

A consequence of the sun synchronous orbit of Aristoteles is the loss of polar coverage in an area with a diameter of $2 \times 6.33°$ around both poles whereas, from a geodetic point of view, 90° inclination is preferable. Most global gradiometer error analysis studies, like those of (Colombo,1988) and (Rapp,1988), assume a complete coverage or $I = 90°$ whereas this is not likely to be the case in an actual gradiometer mission. It will be shown that a polar gap of 12.66° in diameter is resulting in a poorly posed problem when one aims for a complete gravity field recovery up to say degree and order 360.

2.3 Error sources

There are various error sources playing a role in gradiometry. The following subsections will discuss the influence of orbit errors, rotational accelerations, non-conservative forces, misalignment and self gravitation on the gradiometer.

2.3.1 Orbit errors

As the gradiometer is observing some or more components of the tensor of second order derivatives, an error is introduced due to the fact that the orbit, and therefore the position of the instrument at a given epoch, can be modeled only up to a certain accuracy. One can only assume that the gradiometer performed its measurements on some computed orbit whereas in reality tensor components are observed on the actual orbit. Orbit errors are mostly caused by errors in force models [such as the gravity field, atmospheric drag, radiation pressure and tidal models] which are required for the computation of the trajectory of the satellite. In this section we will discuss the relation between those forces and the corresponding perturbations of the gradiometer satellite. We will not discuss orbit errors due to a limited tracking coverage or problems inherent to certain ground based tracking systems as described in (Marsh et al.,ibid) since they fall outside the scope of this study.

Perturbations in near circular orbits due to disturbing [or unmodeled] forces acting on the spacecraft are approximated by the Hill equations which are derived in e.g. (Schrama,1989a):

$$\begin{aligned} f_u &= \ddot{u} - 2n_0\dot{v} - 3n_0^2 u \\ f_v &= \ddot{v} + 2n_0\dot{u} \\ f_w &= \ddot{w} + n_0^2 w \end{aligned} \tag{2.3}$$

where u, v and w represent radial, along- and cross-track components of the orbit error, n_0 the mean motion of the spacecraft in a circular reference orbit and where f_u, f_v and f_w symbolize disturbing accelerations acting on the satellite. There exist exact solutions of these differential equations which are homogeneous, particular non-resonant and resonant.

The homogeneous solution of the Hill equations is found by solving eqns. (2.3) for $f_u = f_v = f_w = 0$. This solution describes the effect of initial state vector errors on the orbit cf Kaplan (1976):

$$\begin{aligned} u(t) &= a_u \cos nt + b_u \sin nt + c_u \\ v(t) &= a_v \cos nt + b_v \sin nt + c_v + d_v t \\ w(t) &= a_w \cos nt + b_w \sin nt \end{aligned} \tag{2.4}$$

where the constants a_u through b_w are defined by the initial position and velocity errors at a given reference time.

The particular solutions describe the case where there are forcing functions, here chosen as Fourier series, in the problem. The non-resonant particular solution is found by solving:

$$\begin{aligned} P_u \cos \omega t + Q_u \sin \omega t &= \ddot{u} - 2n_0\dot{v} - 3n_0^2 u \\ P_v \cos \omega t + Q_v \sin \omega t &= \ddot{v} + 2n_0\dot{u} \\ P_w \cos \omega t + Q_w \sin \omega t &= \ddot{w} + n_0^2 w \end{aligned} \tag{2.5}$$

where P_u through Q_w symbolize *time independent* constants. The solution of this system of equations becomes:

$$\begin{aligned} u(t) &= \frac{\omega P_u - 2n_0 Q_v}{\omega(n_0^2 - \omega^2)} \cos \omega t + \frac{\omega Q_u + 2n_0 P_v}{\omega(n_0^2 - \omega^2)} \sin \omega t \\ v(t) &= \frac{(3n_0^2 + \omega^2)P_v + 2n_0 \omega Q_u}{\omega^2(n_0^2 - \omega^2)} \cos \omega t + \frac{(3n_0^2 + \omega^2)Q_v - 2n_0 \omega P_u}{\omega^2(n_0^2 - \omega^2)} \sin \omega t \\ w(t) &= \frac{P_w}{(n_0^2 - \omega^2)} \cos \omega t + \frac{Q_w}{(n_0^2 - \omega^2)} \sin \omega t \end{aligned} \tag{2.6}$$

showing that singularity occurs where the denominator becomes zero which is the case when $\omega = 0$ or $\omega = \pm n_0$. These cases require separate, so-called resonant, solutions which are described in more detail in (Schrama,1989a). The non-resonant particular solution of the Hill equations behaves as a so-called linear system meaning that disturbing force functions (the input of the linear system) and perturbations in the orbit (the corresponding output) occur at the same frequency of $\frac{\omega}{2\pi}$ Hz. Characteristic is the damping behavior with respect to ω of the non-resonant solutions which is caused by the denominators $\omega(n_0^2 - \omega^2)$, $\omega^2(n_0^2 - \omega^2)$ and $(n_0^2 - \omega^2)$ in eqns. (2.6). Therefore orbital perturbations occur mostly in the lower frequency band between approximately 0 and 3 cycles per revolution as is confirmed by various studies such as an orbit error simulation described in (Schrama,1989a).

A similar damping behavior with respect to frequency can be expected in the gradiometer error signal caused by orbital perturbations. This effect is approximated

by linearizing second order derivatives of the potential function $V = \mu/r$ whereby $r = (x^2 + y^2 + z^2)^{1/2}$. The required third order derivatives take the following form:

$$\frac{\partial^3 V}{\partial x_i \partial x_j \partial x_k} = \mu \left\{ \frac{3x_k}{r^5}\frac{dx_i}{dx_j} - 15\frac{x_i x_j x_k}{r^7} + \frac{3}{r^5}\frac{d}{dx_k}(x_i x_j) \right\}$$

For $x_1 = x$, $x_2 = y$ and $x_3 = z$ this results in the following Taylor expansion:

$$\underbrace{\begin{bmatrix} V_{xx} & V_{xy} & V_{xz} \\ V_{yx} & V_{yy} & V_{yz} \\ V_{zx} & V_{zy} & V_{zz} \end{bmatrix}}_{(x+\Delta x, y+\Delta y, z+\Delta z)} = \underbrace{\begin{bmatrix} V_{xx} & V_{xy} & V_{xz} \\ V_{yx} & V_{yy} & V_{yz} \\ V_{zx} & V_{zy} & V_{zz} \end{bmatrix}}_{(x,y,z)} + \frac{3\mu}{r^4} \begin{bmatrix} \Delta z & 0 & \Delta x \\ 0 & \Delta z & \Delta y \\ \Delta x & \Delta y & -2\Delta z \end{bmatrix} \qquad (2.7)$$

in which one replaces $\Delta x = w$, $\Delta y = v$ and $\Delta z = u$. At 200 km altitude the term $3\mu/r^4$ equals approximately $6.4 \times 10^{-13}\ m^{-1}s^{-2}$ indicating that orbit errors of the order of 10 m are required to obtain the 0.01 E level whereas errors of 0.1 m correspond to 10^{-4} E.

Figure 2.2 shows the results of a simulation cf Bettadpur (1990) in which tensor components are computed as if they occur on a reference and a perturbed trajectory. The amplitude density spectrum of the differences between T_{uu} on both trajectories demonstrates that most of the orbit error problem in the gravity gradients occurs below 4 cpr for a 0.01 E/$\sqrt{\text{Hz}}$ instrument and below 25 cpr for a 0.0001 E/$\sqrt{\text{Hz}}$ instrument. A simple, but efficient, way of avoiding the orbit error problem is therefore to filter the lower part of the frequency spectrum in the error analysis. Other techniques to treat the effect of orbit errors on gravity gradients are cf (Rummel & Colombo, 1985):

- to consider orbit error free combinations such as $2V_{xx} - V_{zz}$ and $2V_{yy} - V_{zz}$,
- to introduce initial state vector components and possibly forcing terms (P_u through Q_w in eq. (2.5)) as unknowns in an estimation problem. [The observation equations for this problem are obtained by substitution of (2.4) and (2.6) in (2.7)].

In this study the former technique, elimination of the lower part of the spectrum, is used to avoid any unnecessary complexity in the error analysis. Various references on the orbit error problem in gradiometry can be found in (Rummel,1986), the technique of filtering originates from (Colombo,1988).

2.3.2 Rotational effects

Any rotation of the gradiometer causes disturbing rotational accelerations which are observed by the instrument. Therefore in the following two subsections we will discuss 1) the effect of angular velocities [ω] and accelerations [$\dot{\omega}$] on the accelerometers [a static approach] and 2) the behavior of ω and $\dot{\omega}$ in time [a dynamic approach].

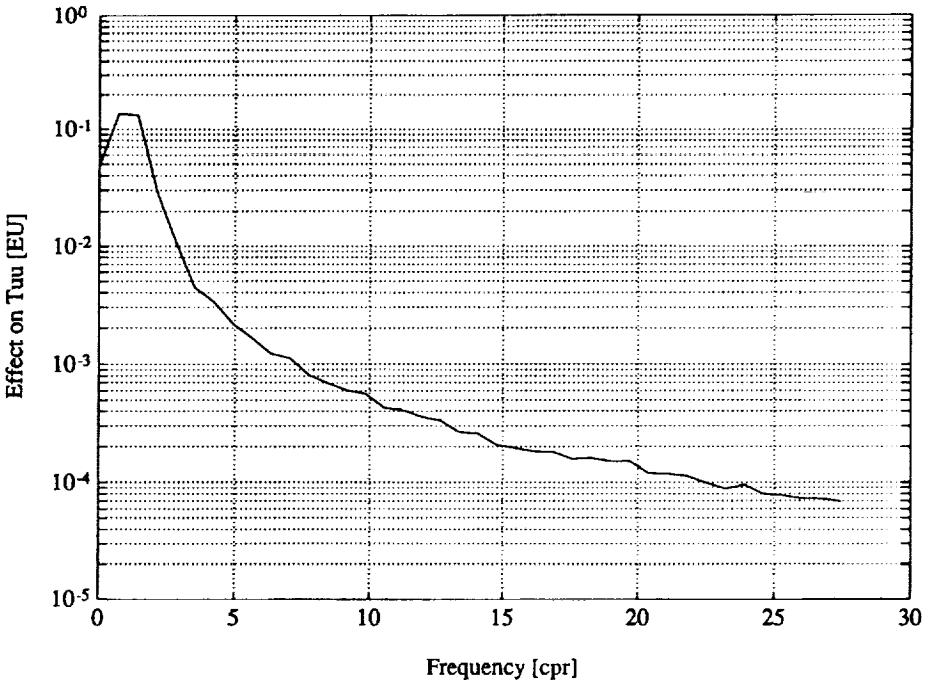

Figure 2.2: Amplitude density spectrum of the error in T_{uu} caused by orbital perturbations. On the horizontal axis the frequency is represented in terms of cycles per revolution with a resolution of 0.7 cpr. On the y-axis the error is presented in terms of E.

Attitude problem, static approach

According to Rummel (1986) any accelerometer will measure the total acceleration $\ddot{\overline{R}}$ which is:

$$\ddot{\overline{R}} = \ddot{\overline{R}}_0 + \overline{\omega} \times \dot{\overline{R}}_0 + \dot{\overline{\omega}} \times \overline{R} + \overline{\omega} \times (\overline{\omega} \times \overline{R}) \tag{2.8}$$

where $\ddot{\overline{R}}_0$ and $\dot{\overline{R}}_0$ describe respectively the acceleration and the velocity of the instrument frame and where $\overline{R}$ equals to the displacement vector relative to the center of mass of the spacecraft. Equation (2.8) can be evaluated for differences in accelerations which are actually observed in the instrument frame whose origin is located at the center of mass of the spacecraft. This results in:

$$\begin{bmatrix} \Delta\ddot{R}_1 \\ \Delta\ddot{R}_2 \\ \Delta\ddot{R}_3 \end{bmatrix} = (\Gamma + \dot{\Omega} + \Omega^2) \begin{bmatrix} \Delta R_1 \\ \Delta R_2 \\ \Delta R_3 \end{bmatrix} \tag{2.9}$$

where $\Delta\overline{R}$ symbolizes the difference of the displacement vector of two accelerometers while Γ symbolizes the tensor of second order derivatives of V:

$$\Gamma = \begin{bmatrix} V_{xx} & V_{xy} & V_{xz} \\ V_{yx} & V_{yy} & V_{yz} \\ V_{zx} & V_{zy} & V_{zz} \end{bmatrix}.$$

Furthermore

$$\dot{\Omega} = \begin{bmatrix} 0 & -\dot{\omega}_3 & \dot{\omega}_2 \\ \dot{\omega}_3 & 0 & -\dot{\omega}_1 \\ -\dot{\omega}_2 & \dot{\omega}_1 & 0 \end{bmatrix}$$

and

$$\Omega^2 = \begin{bmatrix} -\omega_2^2 - \omega_3^2 & \omega_1\omega_2 & \omega_1\omega_3 \\ \omega_1\omega_2 & -\omega_1^2 - \omega_3^2 & \omega_2\omega_3 \\ \omega_1\omega_3 & \omega_2\omega_3 & -\omega_1^2 - \omega_2^2 \end{bmatrix}.$$

For $\Lambda = \Gamma + \dot{\Omega} + \Omega^2$, the tensor which is actually observed by the instrument, we find the following relations:

$$\dot{\Omega} = \frac{1}{2}(\Lambda - \Lambda^T) \tag{2.10}$$

and

$$\Gamma + \Omega^2 = \frac{1}{2}(\Lambda + \Lambda^T). \tag{2.11}$$

In principle, for a 3-axis gradiometer, one could obtain Ω by an integration of $\dot{\Omega}$ with respect to time, cf (Rummel,1986):

$$\Omega(t) = \int_0^t \dot{\Omega}\, dt \; + \; \Omega_0 \; . \tag{2.12}$$

This approach helps to estimate Ω^2 in eq. (2.11) thereby separating rotational from gravitational effects. Unfortunately this technique can not be applied for a 2-axis gradiometer as is the case for Aristoteles. Assuming that axis number 1 is radial, 2 along track and 3 cross track, heading in the same direction as the angular momentum vector of the orbit, we find that the following components can be observed:

$$\begin{aligned} \Lambda_{11} &= \Gamma_{11} - (\omega_2^2 + \omega_3^2) \\ \Lambda_{33} &= \Gamma_{33} - (\omega_1^2 + \omega_2^2) \\ \Lambda_{13}^* &= \frac{1}{2}(\Lambda_{13} + \Lambda_{31}) = \Gamma_{13} + \omega_1\omega_3 \end{aligned} \tag{2.13}$$

Assuming that ω_3 [nominally the mean motion when the spacecraft is designed to fly in an Earth pointing mode] is far larger than ω_1 or ω_2 and ignoring all terms

containing ω_2 since they are estimable by means of eq. (2.10) and (2.12) one can linearize eqns. (2.13) as:

$$\begin{aligned} \Delta\Lambda_{11} &= \Delta\Gamma_{11} - 2n_0\Delta\omega_3 \\ \Delta\Lambda_{33} &= \Delta\Gamma_{33} - 2\omega_1\Delta\omega_1 \\ \Delta\Lambda_{13}^{*} &= \Delta\Gamma_{13} + \omega_1\Delta\omega_3 + n_0\Delta\omega_1 \end{aligned} \tag{2.14}$$

From eqns. (2.14) one can conclude for a $0.01\mathrm{E}/\sqrt{\mathrm{Hz}}$ instrument that $\Delta\omega_1$ and $\Delta\omega_3$ [here symbolizing the yaw and pitch rate] must be known respectively to 10^{-8} and 5×10^{-9} rad/s which poses a severe constraint on the restitution of attitude of the instrument, cf (ESA,1989).

According to this report (ibid) modern gyroscopes obtain an accuracy of 10^{-7} rad/s inside the measurement bandwidth of 5×10^{-3} to 0.125 Hz which is unfortunately still a factor 10 to 20 too large for an adequate attitude reconstruction. Even the inclusion of a star tracker [1 arc second or 4.8×10^{-6} radians is feasible by current space qualified star trackers] in this configuration wouldn't help since the required 10^{-8} rad/s couldn't be obtained in a 4 second integration period which is the sampling time proposed for Aristoteles.

A possible solution, proposed by Matra Espace cf (ESA,1989), is to predict with existing gravity models values of Γ_{13} to within 0.5 E in order to improve the estimation of ω_1 and ω_3 thereby enabling to derive more accurately Γ_{11} and Γ_{33}. This seems to be possible since the differences of T_{uw} computed by two existing high degree and order gravity models seem to be smaller than the required 0.5 E, cf (Schrama,1989b). However in this technical memorandum (ibid) we warned that both models share mostly the same observations [mostly gravity anomalies] so that the statistics are obscuring the real accuracy of Γ_{13}. With this in mind Matra's proposal leads to a vicious circle where one builds a gradiometer to measure a high degree and order gravity field which happens to operate only when an a priori model of such a field exists.

The above mentioned problems were a good reason to consider the attitude problem in a dynamic approach [considering differential equations] in an attempt to describe $\Delta\omega_i$ as functions of the time caused by disturbing torques. Such an approach explains the behavior of the rotational velocity components in the frequency domain as is shown in the following section.

Attitude problem, dynamical approach

The Newton-Euler equations take the following form:

$$\dot{\overline{H}} = -\overline{\omega} \times \overline{H} + \overline{T} \tag{2.15}$$

where $\overline{H}$ is equal to the angular momentum vector, $\overline{\omega}$ is a polar vector containing angular velocities and $\overline{T}$ is a torque vector. By definition, $\overline{H} = I\overline{\omega}$, where I is a

tensor containing the moments of inertia of the body under consideration. As a result the Newton-Euler rotational equations take the following form:

$$I\dot{\overline{\omega}} = -\overline{\omega} \times I\overline{\omega} + \overline{T} \tag{2.16}$$

These equations are considered in the case where I represents a diagonal matrix containing the principle axes of inertia:

$$\begin{aligned} I_1\dot{\omega}_1 &= (I_2 - I_3)\omega_2\omega_3 + T_1 \\ I_2\dot{\omega}_2 &= (I_3 - I_1)\omega_1\omega_3 + T_2 \\ I_3\dot{\omega}_3 &= (I_1 - I_2)\omega_1\omega_2 + T_3 \end{aligned} \tag{2.17}$$

In our case we know that Aristoteles is in an Earth pointing mode and that the torques are caused by a combination of gravitational torques, control torques needed for attitude control [momentum wheels], and other torques which are mainly due to the atmospheric drag acting on the satellite. Some insight can be gained by linearizing the Newton-Euler equations [including the gravitational torques] for small rotations assuming a nominal rotation about the ω_3 axis [cross-track axis] of the spacecraft. This results in the following system of differential equations as is shown in (Morgan and Paik,1988):

$$\begin{aligned} I_1\ddot{\theta}_1 &= (I_1 + I_2 - I_3)n_0\dot{\theta}_2 + (I_2 - I_3)n_0^2\theta_1 + T_1 \\ I_2\ddot{\theta}_2 &= (I_3 - I_2 - I_1)n_0\dot{\theta}_1 + 4(I_1 - I_3)n_0^2\theta_2 + T_2 \\ I_3\ddot{\theta}_3 &= 3(I_1 - I_2)n_0^2\theta_3 + T_3 \end{aligned} \tag{2.18}$$

Here the variables θ_i symbolize small angles [$\dot{\theta}_i = \omega_i$], whereas T_i symbolizes torques free of gravitational effects. The particular non-resonant solution of (2.18) is obtained by assuming that:

$$\begin{aligned} \frac{T_1}{I_1} &= R_1 \cos\beta n_0 t \\ \frac{T_2}{I_2} &= R_2 \sin\beta n_0 t \\ \frac{T_3}{I_3} &= R_3 \cos\beta n_0 t \end{aligned} \tag{2.19}$$

whereby β is determining the frequency in terms of cycles per revolution. The non-resonant solutions become:

$$\begin{aligned} \theta_1(t) &= \frac{-(\beta^2 + Q_2)R_1 + \beta P_1 R_2}{n_0^2((\beta^2 + Q_1)(\beta^2 + Q_2) + \beta^2 P_1 P_2)} \cos\beta n_0 t \\ \theta_2(t) &= \frac{-(\beta^2 + Q_1)R_2 - \beta P_2 R_1}{n_0^2((\beta^2 + Q_1)(\beta^2 + Q_2) + \beta^2 P_1 P_2)} \sin\beta n_0 t \\ \theta_3(t) &= \frac{-R_3}{n_0^2(\beta^2 + Q_3)} \cos\beta n_0 t \end{aligned} \tag{2.20}$$

whereby

$$P_1 = \frac{I_1 + I_2 - I_3}{I_1}, \quad Q_1 = \frac{I_2 - I_3}{I_1}$$

$$P_2 = \frac{I_3 - I_2 - I_1}{I_2}, \quad Q_2 = \frac{4(I_1 - I_3)}{I_2}$$

$$Q_3 = \frac{3(I_1 - I_2)}{I_3}$$

These solutions describe the behavior of attitude errors as a result of disturbing non-gravitational torques [divided by moments of inertia] which converted to rotational velocities [$\Delta\omega_1 = \dot{\theta}_1$ and $\Delta\omega_3 = \dot{\theta}_3$] and substituted in eqns. (2.14) result in error estimates for $\Delta\Lambda_{ij}$. Note that eqns.(2.20a-b) become singular when:

$$\beta^2 = -\frac{1}{2}(P_1P_2 + Q_1 + Q_2) \pm \frac{1}{2}\sqrt{(P_1P_2 + Q_1 + Q_2)^2 - 4Q_1Q_2} \tag{2.21}$$

and that (2.20c) becomes singular when:

$$\beta^2 = -Q_3. \tag{2.22}$$

This problem is not considered any further, it results in a resonant set of D.E.'s which must be treated separately.

More important is the result that attitude errors, and thereby angular velocities and gradiometer signal errors, are decaying at a rate inversely proportional to the frequency of the disturbing torque function, see also eq.(2.20). Therefore one could expect that attitude errors are confined to the lower frequency band and that the problem could be avoided by means of a high pass filtering technique similar to the way orbital errors are treated. This is discussed in Appendix A where the results of a simulation of attitude errors for a 10^{-2} and a 10^{-4} E gradiometer satellite are shown. Unfortunately the results indicate that the torques caused by atmospheric drag are probably too large for even a 10^{-2} E instrument and that the attitude must be reconstructed to higher accuracies than presently suggested for Aristoteles. Additional studies are needed to determine whether this is feasible with modern processing techniques and or technology resulting in an acceptable solution within the budgetary constraints.

2.3.3 Other effects

So far the effects of orbit errors and rotations have been discussed. There are several other effects causing errors in the gradiometer signal such as misalignment between axes, scale-errors, coupling and non-linearity of the accelerometers, including effects due to self gravitation [fuel sloshing].

Scale, coupling and non-linearity

According to Touboul et al. (1990) the acceleration measured along the i-axis γ_i may be described by:

$$\begin{aligned} \gamma_i \;=\; & (1+\epsilon_i)\Gamma_i \;+\; \epsilon_i^j\Gamma_j \;+\; \epsilon_i^k\Gamma_k \\ & + \epsilon_i^{ii}\Gamma_i\Gamma_i + \epsilon_i^{ij}\Gamma_i\Gamma_j + \epsilon_i^{ik}\Gamma_i\Gamma_k \\ & + \textit{bias} \;+\; \textit{noise} \end{aligned} \tag{2.23}$$

where:

- Γ_i, Γ_j and Γ_k are the sum of all external accelerations projected on the i,j and k-axes,
- ϵ_i is a bias term for the i-axis, e.g. due to an electronic or mechanical bias in the accelerometer,
- ϵ_i^j and ϵ_i^k are the coupling terms between the i,j and k-axis, due to misalignment of the sensitive axis of the accelerometer and the actual frame axis of the gradiometer and obliqueness of axes,
- ϵ_i^{ii}, ϵ_i^{ij} and ϵ_i^{jk} are non-linearity terms which are mainly due to defects of symmetry of the electrostatic suspension system around the accelerometer proof mass.

A complete treatment of the "scale, coupling non-linearity" problem for Aristoteles is described by Touboul et al. (ibid). They mention that in-orbit measurements by means of a calibration device are needed to obtain ϵ_i at $\approx 10^{-5}$ in a relative sense and ϵ_i^j and ϵ_i^k at $\approx 10^{-5}$ rad [which allows atmospheric drag accelerations up to $5 \times 10^{-7}\ m/s^2$].

The principle danger of "scaling, coupling and non-linearity" errors in the gradiometer is that non-conservative external forces, in this case dominated by atmospheric drag, enter directly in the observed signal. The magnitude and spectral behavior of the drag fluctuations are derived from the results obtained from the missions of Castor, Atmosphere Explorer-C and Dynamics Explorer 2 which are also discussed in (Touboul et al.,ibid). They conclude that the velocity vector of the spacecraft must be as perpendicular as possible to the gradiometer plane. This may require a so-called yaw-steering mode of Aristoteles compensating for cross-track winds near the poles, see also (ESA,1989).

Self gravitation

Figure 2.3 is taken from (Morgan & Paik,1988) and shows the expected measurement signal in terms of E due to masses varying from 0.01 to 1000 kg in the range of 0.1 to 100 meter from the gradiometer. It explains that any gradiometer in a spacecraft

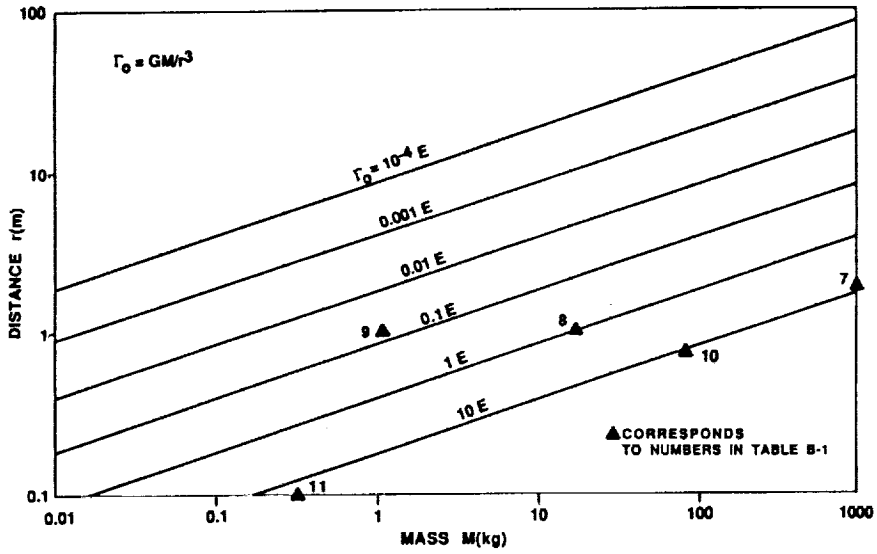

Figure 2.3: Gradient sensitivity level, cf (Morgan and Paik,1988).

is biased to a certain amount by self-gravitation. More serious are masses vibrating at frequencies inside the measurement bandwidth of the gradiometer, implying that care must be taken in the design of antennas and other appendages so that the eigen-frequencies of vibration are outside the measurement bandwidth or alternatively to insure that the magnitude of vibration is too small to be noticed by the instrument. In this context sloshing of fuel should be avoided in the proximity of the instrument requiring a special design of the hydrazine tanks, see also (ESA,1989).

Chapter 3

Gravity field error analysis

3.1 Introduction

The objective for launching a satellite equipped with a gradiometer and a GPS receiver is to improve the Earth's gravity model. The goal of an error analysis is to quantify the expected accuracy of recovered potential coefficients given certain characteristics of the instruments, the orbit and a priori information about the gravitational field.

The next logical step after an error analysis would be to carry out an actual simulation/recovery experiment. In the simulation part of such an experiment, gravity gradients including noise and systematic effects are generated by means of existing models and known characteristics of the spacecraft and instruments; during recovery one attempts to estimate the potential coefficients from the simulated observations.

Undoubtly the latter experiment is more convincing for demonstrating the efficiency of a processing technique. However it is also far more laborious than the error analysis technique described here and therefore an expensive method for studying the effect of assumptions made in the generation part. [The generation part would for instance depend on the availability of a super computer and a good deal of computing time since it consists of evaluating spherical harmonic expressions of gravity gradients up to $l = 360$ along a reference orbit.]

3.1.1 Problem definition

The problem definition assumed here is shortly summarized as follows:

- A circular orbit is assumed, orbital decay, eccentricity effects and C_{20} short periodic oscillations are not considered,
- The inclination of the orbital plane I is fixed during the mission, any choice of I is allowed,

- In the nominal orbit the elements Ω,ω and M are allowed to drift linearily as a result of C_{20} secular gravitational effects,
- It is assumed that the orbit repeat ratio allows the estimation of a gravity field up to a given degree and order,
- Gradiometer observations as well as position estimates from a GPS receiver are used as observation types to model the gravity field,
- Covariance functions of the above mentioned observation types are formulated in the spectral domain and are based upon the accuracy of the instrument, sampling time and the mission duration.

3.2 Error analysis

3.2.1 Lumped coefficient approach

In the error analysis so-called lumped coefficient expressions of gravity gradients and GPS position estimates are used as observation equations. Therefore we discuss the subjects: spherical harmonics along a reference orbit, the requirements for a repeat orbit and the gradiometer and GPS observation equations in the form of lumped coefficient expressions.

Spherical harmonics along a circular orbit

The potential function, including gravity gradients as will be shown later on, expressed in spherical harmonics up to degree and order L projected on the nominal orbit may be written as a Fourier series:

$$T = \sum_{k=-L}^{L} \sum_{m=0}^{L} A_{km} \cos \psi_{km} + B_{km} \sin \psi_{km} \tag{3.1}$$

where A_{km} and B_{km} are so-called lumped coefficients related to the original potential coefficients as, cf (Schrama,1989a):

$$\begin{bmatrix} A_{km} \\ B_{km} \end{bmatrix} = \sum_{l=lmin,2}^{L} \begin{bmatrix} \alpha_{lm} & \beta_{lm} \\ \beta_{lm} & -\alpha_{lm} \end{bmatrix} \begin{bmatrix} H_{lmk} \\ G_{lmk} \end{bmatrix} \tag{3.2}$$

where

$$\alpha_{lm} = \begin{bmatrix} \overline{C}_{lm} \\ -\overline{S}_{lm} \end{bmatrix}_{l-m:odd}^{l-m:even} \quad \wedge \quad \beta_{lm} = \begin{bmatrix} \overline{S}_{lm} \\ \overline{C}_{lm} \end{bmatrix}_{l-m:odd}^{l-m:even}$$

$$H_{lmk} = \frac{\mu}{a_e} \left(\frac{a_e}{r} \right)^{l+1} \overline{F}_{lm(l-k)/2}(I) \quad \wedge \quad G_{lmk} = 0$$

$$lmin = \max(|k|, m) + \delta, \quad \delta = \begin{cases} 0 \text{ when } k - \max(|k|, m) : even \\ 1 \text{ when } k - \max(|k|, m) : odd \end{cases}$$

and

$$\psi_{km} = \psi^0_{km} + \dot{\psi}_{km} t \tag{3.3}$$

where it is assumed that $\dot{\psi}_{km}$ is determined by J_2 secular effects as is discussed in (Kaula,1966a):

$$\dot{\psi}_{km} = k(\dot{\omega} + \dot{M}) + m(\dot{\Omega} - \dot{\theta}) = k\dot{\omega}_o + m\dot{\omega}_e \tag{3.4}$$

Non-overlapping lumped coefficients

A block diagonal system of observation equations is obtained when lumped coefficients for arbitrary values of k and m occur at a unique frequency $\dot{\psi}_{km}/2\pi$ Hz. This convenient property will be used throughout this study and is described in this section.

The actual frequency in cycles per revolution $\beta_{km}[= \dot{\psi}_{km}/\dot{\omega}_o]$ may be written as:

$$\beta_{km} = k + m\frac{\dot{\omega}_e}{\dot{\omega}_o} = k + m\frac{N_d}{N_r} \tag{3.5}$$

where $k \in [-L, L]$, $m \in [0, L]$ and $\{N_d, N_r\} \in \mathcal{N}$ due to the orbit repeat condition. The variables N_d and N_r are respectively the number of nodal days $[2\pi/\dot{\omega}_e$ seconds] and the number of revolutions in a repeat period. In order to prevent overlapping of lumped coefficients one has to avoid:

$$\frac{N_d}{N_r} = \frac{N^\star_d}{N^\star_r} \text{ where } |N^\star_d| < |N_d| \ \wedge \ |N^\star_r| < |N_r| \text{ and } \{N^\star_d, N^\star_r\} \in \mathcal{N}$$

which results in the following conditions:

- N_d can be an arbitrary integer
- N_r must be a prime number.

Secondly one has to avoid:

$$\beta_{k_1 m_1} = \beta_{k_2 m_2} \text{ where } k_1 \neq k_2 \wedge m_1 \neq m_2$$

which is possible for k, m combinations resulting in β_{km} terms which are 180° out of phase so that $\beta_{k_1 m_1} = -\beta_{k_2 m_2}$. According to eq.(3.5) this is the case when:

$$\begin{aligned} c &= k_1 + m_1\frac{N_d}{N_r} \\ -c &= k_2 + m_2\frac{N_d}{N_r} \end{aligned}$$

resulting in:

$$\frac{N_d}{N_r} = -\frac{k_1 + k_2}{m_1 + m_2}.$$

It follows directly that overlapping of β_{km} can be avoided by taking N_r greater than $2L$ since $\max(m_1 + m_2) = 2L$. However overlapping of zonal lumped coefficients can not be prevented since it will always occur for β_{k0} and β_{-k0}.

Both conditions are fulfilled when there are a sufficient number of revolutions in a repeat period [$N_r > 2L$] while N_r is chosen as a prime number. For an actual gravity mission with the objective to solve for a gravity field up to $L = 360$ this means that at least 44.3 days or 721 revolutions are needed in a repeat period.

Gradiometer observation equations

The conventional way of expressing gravity gradients at a point somewhere in the r, ϕ, λ space is discussed by Rummel (1986). In his lecture notes gravity gradients are expressed in terms of derivatives of the potential function with respect to r, ϕ and λ assuming that tensor components are evaluated on a polar orbit. Here these expressions can not be used since gravity gradients are required along an inclined orbital plane.

The expressions used here to relate gravity gradients to partial derivatives of orbital parameters are discussed in Appendix B. By using eqns. (B.6), (B.7), (B.8) and (B.9) one can derive the following H and G terms as they are used in equations identical to (3.2) for lumped coefficients of gravity gradients:

$$H^{uu}_{lmk} = \frac{(l+1)(l+2)}{r^2} H_{lmk} \tag{3.6}$$

$$G^{uv}_{lmk} = -\frac{k(l+2)}{r^2} H_{lmk} \tag{3.7}$$

$$H^{vv}_{lmk} = -\frac{k^2 + (l+1)}{r^2} H_{lmk} \tag{3.8}$$

$$H^{ww}_{lmk} = \frac{k^2 - (l+1)^2}{r^2} H_{lmk} \tag{3.9}$$

For the tensor components T_{uw} and T_{vw} there exist different expressions for the lumped coefficients due to a modulation of $\sin\omega_o$ and $\cos\omega_o$ in eqns. (B.14) and (B.15). In this case the lumped coefficients are related to α_{lm} and β_{lm} as: [$\bullet = u, v$ or w, see Appendix B]

$$\begin{bmatrix} A^{\bullet\bullet}_{km} \\ B^{\bullet\bullet}_{km} \end{bmatrix} = \sum_{l=lmin,2}^{L} \frac{1}{2} \begin{bmatrix} \alpha_{lm} & \beta lm \\ \beta_{lm} & -\alpha_{lm} \end{bmatrix} \begin{bmatrix} H^{\bullet\bullet(c)}_{lmk-1} + H^{\bullet\bullet(c)}_{lmk+1} \\ G^{\bullet\bullet(c)}_{lmk-1} + G^{\bullet\bullet(c)}_{lmk+1} \end{bmatrix} + \frac{1}{2} \begin{bmatrix} \alpha_{lm} & -\beta lm \\ \beta_{lm} & \alpha_{lm} \end{bmatrix} \begin{bmatrix} G^{\bullet\bullet(s)}_{lmk-1} - G^{\bullet\bullet(s)}_{lmk+1} \\ H^{\bullet\bullet(s)}_{lmk-1} - H^{\bullet\bullet(s)}_{lmk+1} \end{bmatrix} \tag{3.10}$$

The G and H terms become

$$H^{uw(s)}_{lmk} = -\frac{(l+2)}{r^2}\frac{\partial H_{lmk}}{\partial I} \tag{3.11}$$

$$G^{uw(c)}_{lmk} = \frac{(l+2)}{r^2}(m\sin^{-1}I - k\frac{\cos I}{\sin I})H_{lmk} \tag{3.12}$$

$$H^{vw(c)}_{lmk} = \frac{k(m-\cos I)}{r^2\sin I}H_{lmk} - \frac{1}{r^2}\frac{\partial H_{lmk}}{\partial I} \tag{3.13}$$

$$G^{vw(s)}_{lmk} = \frac{(k\cos I - m)}{r^2\sin I}H_{lmk} + \frac{k}{r^2}\frac{\partial H_{lmk}}{\partial I} \tag{3.14}$$

GPS observation equations

The GPS observation equations are derived from the non-resonant particular solution of the Hill equations given by eq. (2.6). In the next step ω in this equation is replaced by $\beta_{km}n_0$ and all partial derivatives are substituted [$\bullet = u, v$ or w]:

$$\Delta\bullet(t) = \sum_k\sum_m A^{\Delta\bullet}_{km}\cos\psi_{km} + B^{\Delta\bullet}_{km}\sin\psi_{km} \tag{3.15}$$

The observation equations for u and v become:

$$\begin{bmatrix} A^{\Delta u}_{km} \\ B^{\Delta u}_{km} \end{bmatrix} = \sum_{l=lmin,2}^{L}\frac{\mu}{n_0^2r^2}\left(\frac{a_e}{r}\right)^l\left[\frac{\beta_{km}(l+1)-2k}{\beta_{km}(\beta^2_{km}-1)}\right]\overline{F}_{lm(l-k)/2}\begin{bmatrix}\alpha_{lm}\\ \beta_{lm}\end{bmatrix} \tag{3.16}$$

$$\begin{bmatrix} A^{\Delta v}_{km} \\ B^{\Delta v}_{km} \end{bmatrix} = \sum_{l=lmin,2}^{L}\frac{\mu}{n_0^2r^2}\left(\frac{a_e}{r}\right)^l\left[\frac{2\beta_{km}(l+1)-(\beta^2_{km}+3)k}{\beta^2_{km}(\beta^2_{km}-1)}\right]\overline{F}_{lm(l-k)/2}\begin{bmatrix}\beta_{lm}\\ -\alpha_{lm}\end{bmatrix} \tag{3.17}$$

For w we find:

$$\begin{bmatrix} A^{\Delta w}_{km} \\ B^{\Delta w}_{km} \end{bmatrix} = \sum_{l=lmin,2}^{L}\left[\frac{G^c_{lmk-1}+G^c_{lmk+1}-H^s_{lmk-1}+H^s_{lmk+1}}{2n_0^2(1-\beta^2_{km})}\right]\begin{bmatrix}\beta_{lm}\\ -\alpha_{lm}\end{bmatrix} \tag{3.18}$$

with

$$G^c_{lmk} = \frac{(k\cos I - m)}{r\sin I}H_{lmk} \tag{3.19}$$

$$H^s_{lmk} = \frac{1}{r}\frac{\partial H_{lmk}}{\partial I} \tag{3.20}$$

3.2.2 Normal equations

The system of observation equations:

$$\overline{y} = A\overline{x} + \overline{\epsilon} \tag{3.21}$$

is formed from a combination of gradiometer and the GPS observation equations derived in the previous sections. [namely eq.(3.2) using H_{lmk} and G_{lmk} terms according to eqns. (3.6) through (3.9) and eq.(3.10) through (3.14) for gradiometry and (3.15) through (3.20) for GPS.] [The vector $\overline{y}$ contains the observations in the form of lumped coefficients, the vector $\overline{x}$ contains unknowns for $\overline{C}_{lm}$ and $\overline{S}_{lm}$.] The A matrix, containing the partial derivatives of the lumped coefficients with respect to the unknowns, is block diagonal [one block per order m] provided that the repeat ratio of the reference orbit is chosen such that there is a non overlapping lumped coefficient configuration. In a least squares approach [minimizing $\overline{\epsilon}^T Q_{yy}^{-1} \overline{\epsilon}$] the normal equations become:

$$\hat{x} = (A^T Q_{yy}^{-1} A)^{-1} A^T Q_{yy}^{-1} \overline{y} \tag{3.22}$$

where $N = A^T Q_{yy}^{-1} A$ is called the normal matrix and where Q_{yy} is a covariance matrix of the observations which is considered to be diagonal. In this case N is also block diagonal so that the algorithm for building up and inverting the entire normal matrix is a sequential process in which each block is treated individually.

It is well known that the inverse of the normal matrix equals the covariance matrix of the estimated parameters as is discussed in e.g. (Schrama,1989a). As a result, the diagonal elements of N^{-1} are the estimated variances of potential coefficients which are derived from the observation equations used to build the normal matrix. In the error analysis described here these diagonal elements are used for computing the r.m.s. values per degree of potential coefficients, gravity anomalies and geoid heights as will be discussed later on.

A priori observation variance model

The diagonal Q_{yy} matrix mentioned in the previous section contains the a priori variances of the observations [on the main diagonal] which are in our case the lumped coefficients [for GPS position as well as gradiometer observation equations]. The variance to assign per lumped coefficient depends on the instrument accuracy σ_I, the sampling time Δt and the total length in time over which the samples are taken T [also referred to as the mission duration]. Here it is assumed that σ_I represents a r.m.s. value of all samples in the set of observations. By propagation of variances one can show that:

$$\sigma_0 = \sigma_I \left(\frac{\Delta t}{T} \right)^{1/2} \tag{3.23}$$

where σ_0 equals to the individual r.m.s. per sample. If one assumes that there exists a uniform flat noise spectrum for the observations and that lumped coefficients are obtained from the Fourier transformation of the observation sequence then σ_0 equals to the r.m.s. per lumped coefficient [due to Parceval's identity].

Unfortunately, the total noise spectrum for the gradiometer is not flat; instead it is band limited from 5×10^{-3} to 0.125 Hz, cf (ESA,1989), meaning that (3.23) may

be applied only inside this frequency band. In order to simulate the attitude error problem a $1/\beta$ behavior is assumed for the r.m.s. between 4 and 27 cpr, [$\beta_{min} = 27$ cpr corresponds to 5×10^{-3} Hz.] Accordingly the r.m.s. below 27 cpr is modeled as $(\beta_{min}/\beta) \times \sigma_0$; below 4 cpr an infinite r.m.s. is assumed to avoid the "orbit problem" in the error analysis [see Chapter 2].

In a so-called best case analysis the noise spectrum of GPS position observations is considered to be flat using eq.(3.23). In the worst case Smith et al. (1988) mention that frequencies which are multiples of once per revolution modulated by multiples of once per 12 hours again modulated by multiples of once per day, are omitted in the observation noise spectrum. The rationale is that 1) frequencies which are multiples of once per revolution are caused by failing to solve properly for the trajectory of the low orbiter due to various error sources in the GPS system, 2) frequencies which are multiples of once per 12 hours are caused by orbit errors of the GPS satellites and 3) orbits for Aristoteles are computed once per day. Therefore, in the worst case, frequencies are omitted, or at least down weighted by a certain factor, at $k + m(\omega_e/\omega_o)$ cpr where $|k| \leq 5$ and $m \leq 5$.

Some remarks

There are some characteristics of N^{-1} due to the choice of the Q_{yy} matrix and the structure of the observation equations. In the following it is assumed that the design matrix A only consists of observation equations which are computed with the same values for a_e, r and μ and that Q_{yy} is defined for only one observation type. If one assumes white noise then σ_0 in (3.23) is a **scaling factor** for a unit matrix since $Q_{yy} = \sigma_0 I$. Accordingly:

$$N^{-1} = (A^T(\sigma_0 I)^{-1}A)^{-1} = \sigma_0(A^T A)^{-1} \tag{3.24}$$

which shows that N^{-1} is simply scaled by parameters determining σ_0 [which are the instrumental accuracy σ_I, the sampling time Δt and the mission duration T]. Secondly the problem of variation of r in the error analysis is predictable since all columns in the A matrix are scaled by a factor $(a_e/r)^{l+1}$. As a result any variation of these parameters is nothing more than post multiplication of the orginal A matrix by a diagonal matrix D containing on the main diagonal values scaling the columns.

$$A^* = AD \quad \Rightarrow$$

$$(A^*)^T Q_{yy}^{-1}(A^*) = D^T(A^T Q_{yy}^{-1}A)D \quad \Rightarrow$$

$$(N^*)^{-1} = ((A^*)^T Q_{yy}^{-1}(A^*))^{-1} = D^{-1}N^{-1}D^{-1}$$

showing that N^{-1} is simply pre and post multiplied by D^{-1}. A diagonal element at row i and column i of the inverted normal matrix becomes:

$$(N^*)_{ii}^{-1} = N_{ii}^{-1}D_{ii}^{-2}$$

indicating that a second inversion of N may be avoided.

The drag problem

The drag problem in relation to the instrument scaling is much harder to simulate in an a priori variance spectrum. Atmospheric density data that is available comes from Cactus [elliptic orbit, perigee at 270 km], Dynamics Explorer 2 [elliptic orbit, perigee at 270 km] and Atmosphere Explorer-C [circular orbit at about 250 km], cf Touboul et al (1990). They show that the atmospheric density strongly depends on 1) the geomagnetic index K_p, 2) the latitude [since fluctuations are a factor of 2 to 3 larger at high latitudes than at equatorial latitudes] and 3) whether density data is taken at night or during the day. An important conclusion is that fluctuations are significantly smaller between 0.1 and 0.01 Hz [580...58 cpr] than between 0.01 and 0.005 Hz [58..27 cpr] and below [< 27 cpr].

The easiest way to simulate a drag problem is to apply high pass filtering to the gradiometer spectrum above 27 cpr. This is pursued in one of the simulations at the end of this Chapter. This simulation is supposed to represent a worst case drag situation for Aristoteles as it denies the existence of any lumped coefficient below 27 cpr whereas it is more likely that a degraded gravity gradient signal is observed in this frequency band.

Constrained least squares solutions

Some of the results that will be discussed at the end of this Chapter depend on a priori covariance information for the unknowns involved in the problem. Consider the constrained least squares problem:

$$\bar{y} = A\bar{x} + \bar{\epsilon}_1 \tag{3.25}$$

$$\bar{c} = I\bar{x} + \bar{\epsilon}_2 \tag{3.26}$$

where eq.(3.26) are constraints to direct the unknowns $\bar{x}$ to some a priori vector $\bar{c}$ and where I equals to a unit matrix. The solution for this problem is:

$$\hat{x} = (A^T Q_{yy}^{-1} A + K^{-1})^{-1}(A^T Q_{yy}^{-1}\bar{y} + \bar{c}) \tag{3.27}$$

where K equals to the a priori covariance matrix of the constraints $\bar{c}$ in the problem. The K matrix describes the a priori covariances of the unknowns $\bar{x}$ which are supposed to be centered on the constraints $\bar{c}$. Sometimes the constrained least squares problem for $\bar{c} = \bar{0}$ is referred to as a hybrid norm minimization [or collocation] problem since (3.27) is the minimum of:

$$\bar{\epsilon}^T Q_{yy}^{-1}\bar{\epsilon} + \bar{x}^T K^{-1}\bar{x} \tag{3.28}$$

cf (Schrama,1989a). Here a priori information is used for the potential coefficients where K is assumed to be diagonal. The diagonal contains for the a priori r.m.s. per coefficient:

$$\sigma_{lm} = \frac{1}{2}\sqrt{2}\left(\frac{10^{-5}}{l^2}\right) \tag{3.29}$$

cf (Kaula,1966b). In the algorithm, application of a priori information of the unknowns is performed by adding σ_{lm}^{-2} to the diagonal elements of the least squares normal matrix.

3.2.3 Presentation

After inversion of the normal matrix the so-called variance per coefficient per degree δ_l^2 is computed as:

$$\delta_l^2 = \sum_{m=0}^{l} \frac{\sigma^2\left(\overline{C}_{lm}\right) + \sigma^2\left(\overline{S}_{lm}\right)}{2l+1} \tag{3.30}$$

where $\sigma^2\left(\overline{C}_{lm}\right)$ and $\sigma^2\left(\overline{S}_{lm}\right)$ symbolize the diagonal elements of the inverted normal matrix at the location of $\overline{C}_{lm}$ and $\overline{S}_{lm}$. The following conversions of δ_l exist in order to obtain the degree variance spectra of geoid heights:

$$\delta_l^2(N) = a_e^2 \beta_l^2(\alpha)\delta_l^2 \tag{3.31}$$

and gravity anomalies:

$$\delta_l^2(\Delta g) = \left(\frac{\mu}{a_e^2}\right)^2 (l-1)^2 \beta_l^2(\alpha)\delta_l^2 \tag{3.32}$$

where $\beta_l(\alpha)$ is a smoothing operator with α determining the block spacing on a sphere for the degree variance expressions of gravity anomalies and geoid heights as is described in (Katsambalos,1979).

3.3 Results

3.3.1 Gradiometer only results

Figure 3.1 shows δ_l for all gradiometer components up to degree and order 90 in a so-called ideal case for Aristoteles. This analysis shows that T_{uu} is consistently the most valuable component followed by the off-diagonal terms T_{uv}, T_{uw} and T_{vw}, and the remaining diagonal terms T_{vv} and T_{ww}.

The effect of a limited bandwidth of the gradiometer due to 1) orbit errors, 2) attitude problems, and 3) thermal noise effects is shown in figure 3.2. This analysis shows that limited bandwidths of the gradiometer seriously affect the outcome of

an error analysis. Especially the lower degrees and orders of the gravity solution deteriorate rapidly when limiting the lower end of the noise spectrum.

It was recognized for the gradiometer and the GPS position observation equations that the choice of the inclination of the orbital plane plays an important role. This problem is illustrated in figure 3.3. It was found that these results strongly depend on the value of L [here 120] in the error analysis which is also confirmed by error analyses of the Aristoteles gradiometer done by (Koop et al.,1989).

3.3.2 GPS only results

Typically the mean r.m.s. per coefficient per degree [δ_l] derived from gradiometer observation equations shows a weak improvement in the lower degree and orders [especially in the case where bandwidths are restricted], an optimum sensitivity [a minimum] near $l \approx 70$ and an exponential deterioration beyond this point as is shown in figure 3.2. The best case "GPS only" results appear to show that the lowest degrees and orders are most sensitive followed by a steady exponential deterioration toward higher degrees. Examples for GPS on Aristoteles, Gravity probe-B, and Topex, are shown in figure 3.4.

These simulations indicate that gravity fields can be improved up to degree and orders around 35, 55 and 85 from GPS derived position information on Topex, GP-B and Aristoteles since δ_l intersects Kaula's rule of thumb at these degrees. The corresponding cumulative 1° r.m.s. values for geoid heights and gravity anomalies are shown in figures 3.5 and 3.6. The accuracies in terms of geoid heights and gravity anomalies look very promising especially in the lower degrees and orders.

The best and worst cases for GPS on Aristoteles are shown in 3.7 indicating a deterioration in the lower degrees and orders; in the worst case a priori standard deviations for lumped coefficients at $|k| \leq 5$ and $m \leq 5$ are upgraded by a factor 1000.

3.3.3 GPS only results, constrained least squares approach

Figure 3.8 shows δ_l for Topex, using a least squares approach, assuming $I = 65°$ [case 1] and $I = 90°$ [case 2]. The results for $I = 65°$ indicate that a gravity model solved from Topex GPS data alone should not exceed $l \approx 15$ where it intersects Kaula's rule of thumb.

In contrast to this result a Topex type of satellite at $I = 90°$ would allow to solve for a gravity model up to $l \approx 35$. Case 3, 4 and 5 in figure 3.8 show the $I = 65°$ results now adding the matrix αK^{-1} [α is a regularization factor for weighting a priori information on the coefficients] to the normal matrix for $\alpha = 1$, $\alpha = 0.1$ and $\alpha = 0.01$ respectively. We conclude that:

1. The results for $I = 90°$ are in any case preferable to those at other inclinations. This configuration allows one to solve for a gravity model entirely from one

observation type coming from one satellite. This is a unique situation since most satellite gravity models developed up to now are always "assembled" from several orbiters at various inclinations, heights and eccentricities as is described for the GEM-T2 model in (Marsh et al.,1989),

2. The results for $I = 65°$ show that some a-priori information is needed to obtain a gravity solution comparable to the $I = 90°$ results since a cross-over occurs with "Kaula's rule of thumb" at $l = 35$ between $\alpha = 0.1$ and $\alpha = 0.01$,

3. The $\alpha = 1$, $I = 65°$ collocation solution shows the same characteristics as the solutions presented by (Pavlis et al.,1989), δ_l can not intersect the a priori signal curve [a natural property of a Wiener/Kolmogorov type of estimator] and it appears that the signal to noise ratio is greater than or equal to 1,

4. As a direct result of the previous two statements one can conclude that the signal to noise ratio above degree 25 is dominated by the choice of α.

3.3.4 Gradiometer combined with GPS

Least squares solutions

The most promising results in terms of the mean r.m.s. per coefficient per degree [δ_l] are obtained by combining the GPS and gradiometer observation equations as is shown in figure 3.9 for l up to 300. In this figure case 1 is the gradiometer only solution for Aristoteles, case 2 is the best case GPS solution and case 3 is the combination of both solutions. It is estimated that the signal to noise ratio for such solutions become equal at degree and order 240.

Figure 3.10 and 3.11 show the results of gradiometer only and gradiometer with GPS solutions converted to point, 1° and 5° mean cumulative geoid and gravity anomaly errors. We conclude that: 1) GPS and gradiometer derived solutions are complementary, 2) errors in geoid heights are governed particulary by uncertainties in the lower degree and orders of the gravity field, 3) the original Aristoteles mission objectives [$\epsilon(\Delta g) < 5$ mgal and $\epsilon(N) < 10$ cm at $\lambda = 100$ km] are hard to meet [or maybe even impossible to meet] without the availability of GPS as a tracking facility for Aristoteles and that 4) without the availability of GPS the objectives are easier met for Δg than N.

Hybrid norm solutions

Figure 3.12 shows the results in terms of the mean r.m.s per coefficient per degree obtained by combining the GPS and gradiometer observation equations for l up to 360 pursuing the hybrid norm approach where the full K^{-1} matrix is added to the normal matrix.

Curve 1 in figure 3.12 may be considered as a worst case Aristoteles solution at $I = 96.33°$ assuming that the atmospheric drag problem prohibits the gradiometer to measure any lumped coefficient below 27 cpr. However this solution also depends quite heavily on a GPS solution to L=120. Similar solutions to lower L in the GPS part revealed unsatisfactory large discontinuities in δ_l whereas the degree and order 120 case seemed to be an optimum although still some small jump can be seen.

Curve 2 in figure 3.12 is a best case Aristoteles solution assuming that below 27 cpr deteriorated gravity gradients are observed. A simultaneous solution already gave satisfactory results when GPS observation equations are added to $L = 80$ [a small jump is still observed at $L = 80$] and assuming a hybrid norm solution. In general one may conclude that this procedure results in a somewhat stronger gravity field solution between l=15 and 120 than the previous case.

However both solutions show that the inclination problem [a slightly non-polar orbit] and the bandwidth problem may be avoided by adding GPS observation equations up to sufficient high degree and order and pursuing a hybrid norm approach.

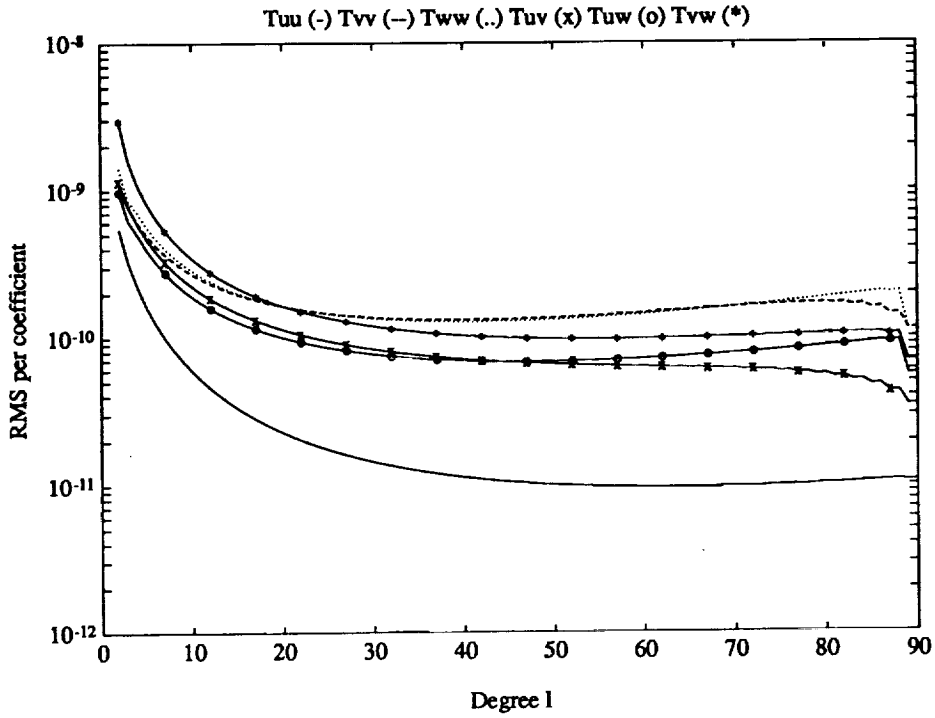

Figure 3.1: Behavior of the gradiometer components T_{uu}, T_{vv} and T_{ww} and T_{uv}, T_{uw} and T_{vw}. [h = 200 km, e = 0.001, I = 90°, no bandwidth restrictions, a sampling time of 4 s, a mission duration of 6 months, 0.01 E instrument precision, least squares solution].

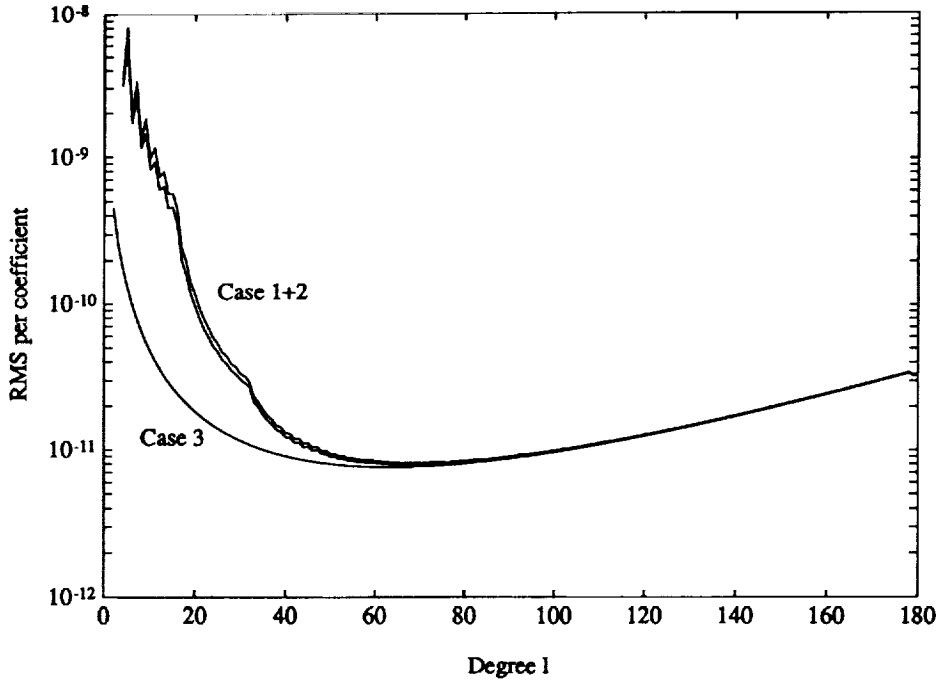

Figure 3.2: Effects of limited bandwidths of the 2-axis gradiometer on Aristoteles. Case 1: lumped coefficients are considered for $4 < \beta < \infty$, below 27 cpr a $1/\beta$ behavior is assumed in the observation noise spectrum. Case 2: assuming a flat noise spectrum for $4 < \beta < \infty$. Case 3: no bandwidth limitations. Common parameters used in all cases are: $h = 200$ km, $e = 0.001$, $I = 90°$ and a mission duration of 6 months, 0.01 E instrumental noise, 4 s sampling time, for T_{uu}, T_{ww} and T_{uw}.

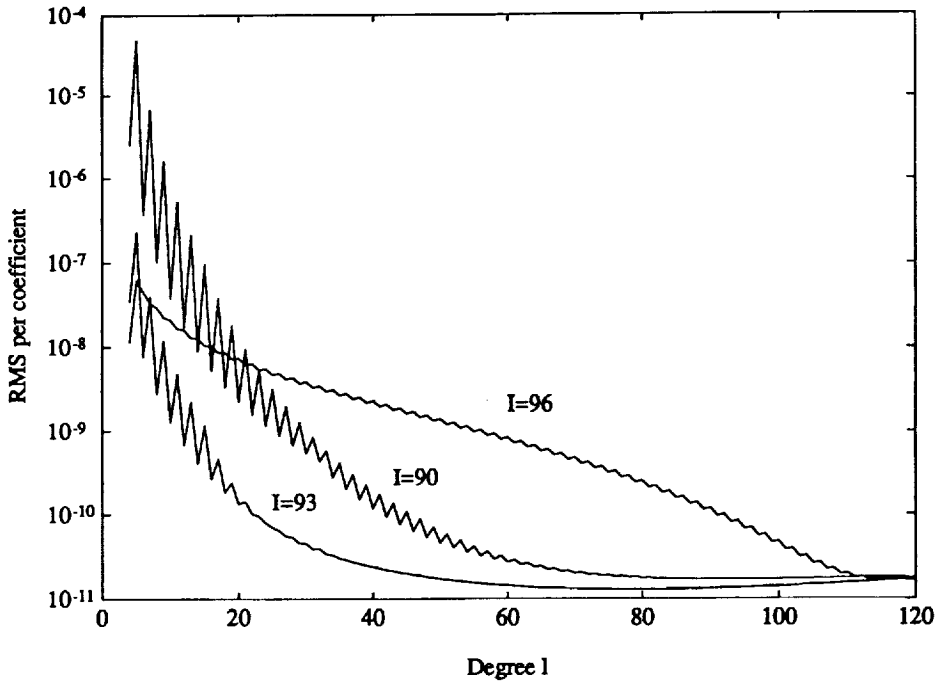

Figure 3.3: The r.m.s per coefficient per degree derived from T_{uu} for $I = 90°$, $93°$ and $96°$ at $h = 200$ km. The mean r.m.s. per coefficient per degree is computed using a least squares approach for T_{uu} assuming $4 < \beta < \infty$, a $1/\beta$ behavior below $\beta_{min} = 27$ cpr, a sampling time of 4 s and mission duration of 6 months.

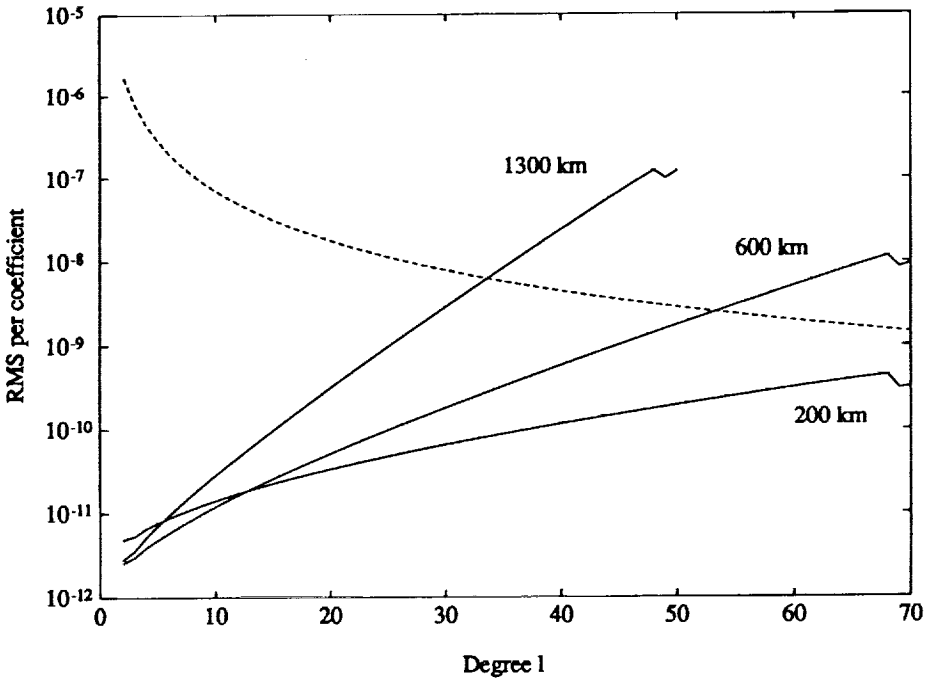

Figure 3.4: The r.m.s. per coefficient per degree using GPS radial, cross – and along track variations for $h = 200$, 600 and 1300 km at $I = 90°$ assuming 3 cm instrumental noise, a sampling time of 1 s and a mission duration of 6 months for Aristoteles and mission duration of 24 months for Topex and GP-B.

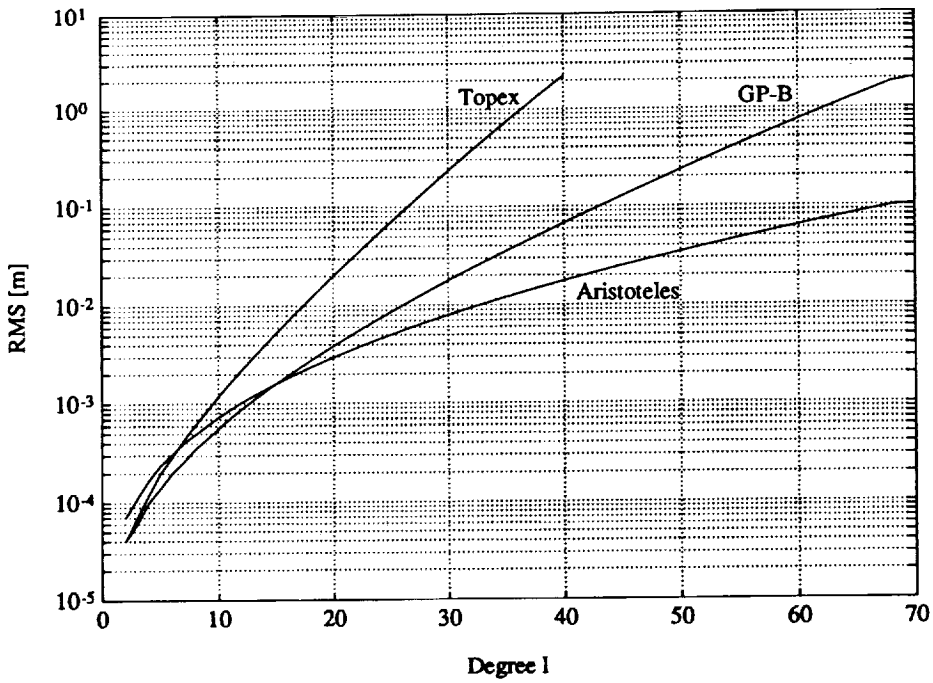

Figure 3.5: Cumulative 1° mean r.m.s. values for geoid heights per degree for GPS on Aristoteles, GP-B and Topex derived from the results show in fig. 3.4.

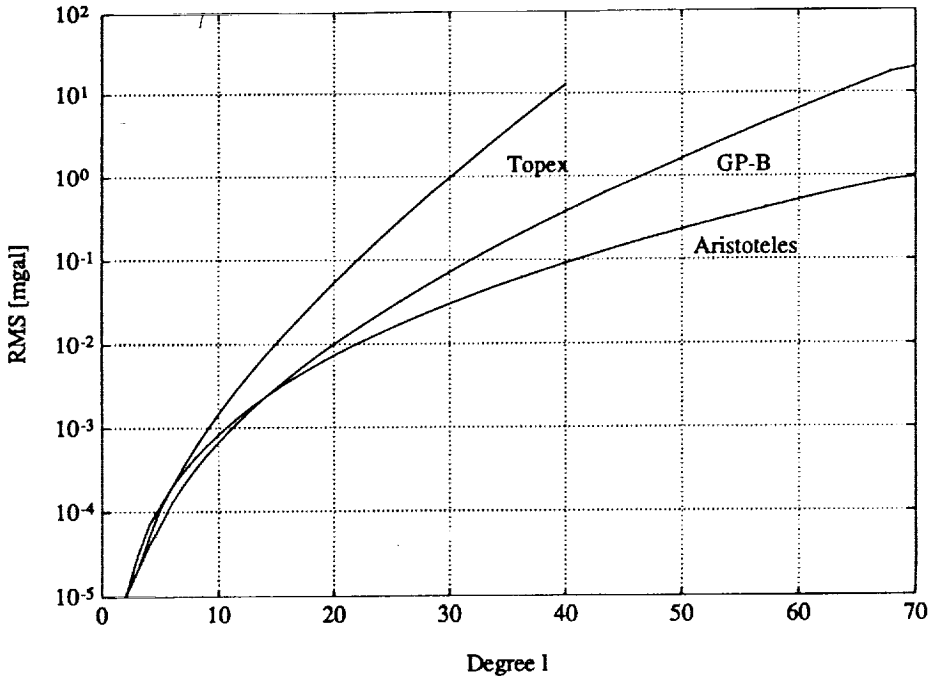

Figure 3.6: Cumulative 1° mean r.m.s. values for gravity anomalies per degree for GPS on Aristoteles, GP-B and Topex derived from the results show in fig. 3.4.

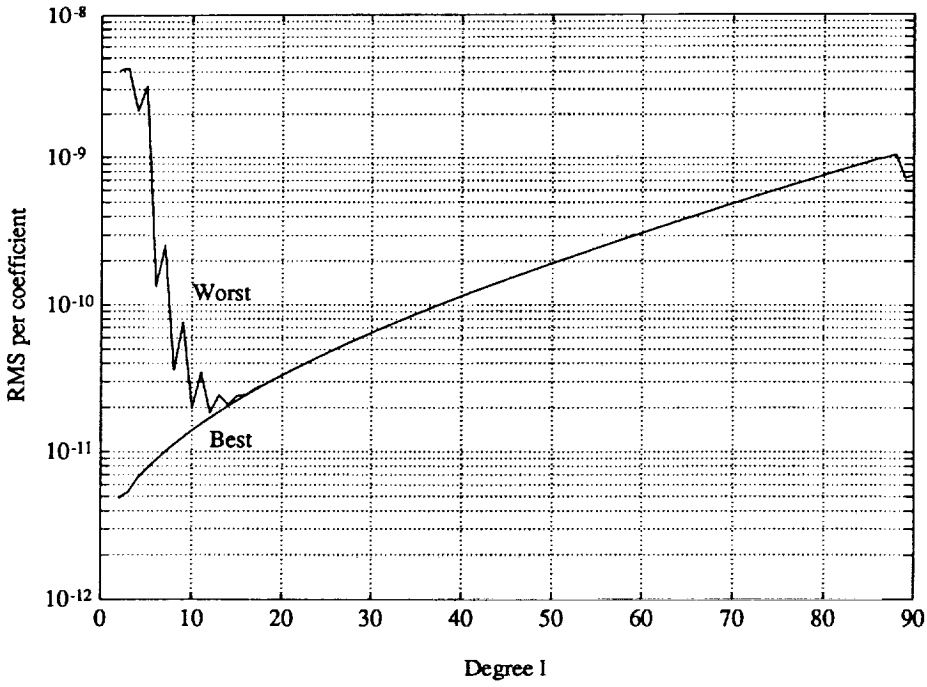

Figure 3.7: The r.m.s. values per coefficient per degree in the GPS best and worst case on Aristoteles. In the best case all lumped coefficients are used, in the worst case lumped coefficients are down weighted a factor 1000 at $|k| \leq 5$ and $|m| \leq 5$.

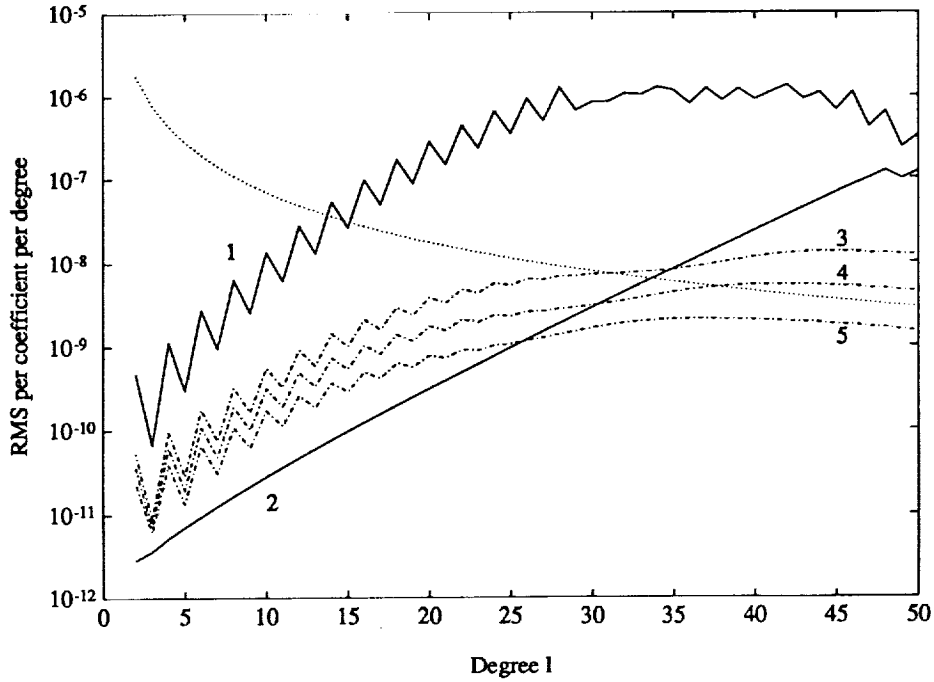

Figure 3.8: The r.m.s. values per coefficient per degree derived from Topex [GPS] best case collocation solutions. Here α is a regularization factor for weighting a priori information on the potential coefficients. Case 1: $I = 65°$. Case 2: $I = 90°$. Case 3: $I = 65°$, $\alpha = 0.01$. Case 4: $I = 65°$, $\alpha = 0.1$. Case 5: $I = 65°$, $\alpha = 1$. In all cases we assumed an instrumental precision of 3 cm, a sampling time of 1 s, a mission duration of 24 months at an altitude of 1300 km for radial, cross – and along track components.

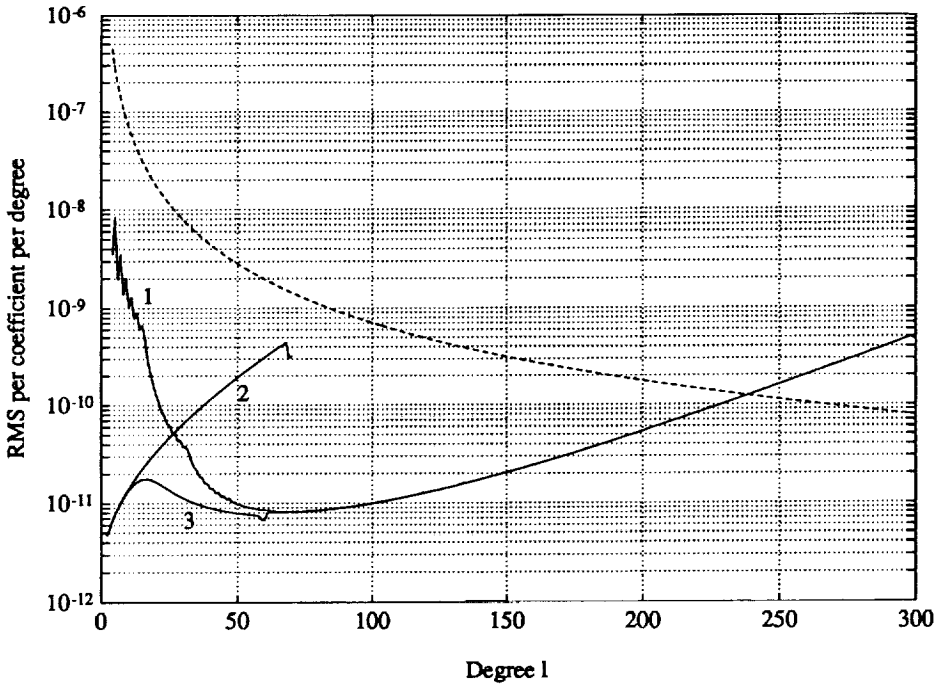

Figure 3.9: The r.m.s. values per coefficient per degree for various individual and combined GPS and gradiometer solutions. All solutions assume a least squares approach and $I = 90°$ and a mission duration of 6 months. Case 1: Gradiometer only solution: we assumed $4 < \beta < \infty$, $\beta_{min} = 27$ cpr, 4 s sampling time and 0.01 E instrumental noise for T_{uu}, T_{uw} and T_{ww}. Case 2: GPS only solution: we assumed $0 < \beta < \infty$, 1 s sampling time and 3 cm instrumental noise for radial, cross – and along track components. Case 3: The combined solution of case 1 and 2.

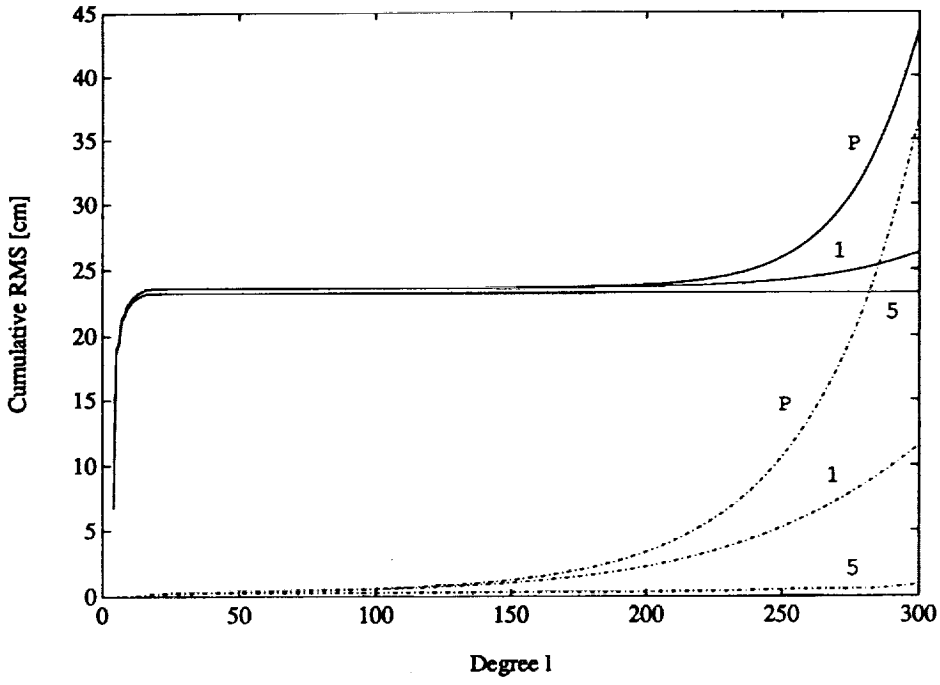

Figure 3.10: The cumulative point, 1° and 5° mean $\delta_l(N)$ values for combined GPS and gradiometer solutions. Dashed: with GPS, solid: without GPS. These values are derived from cases 1 and 3 shown in figure 3.9.

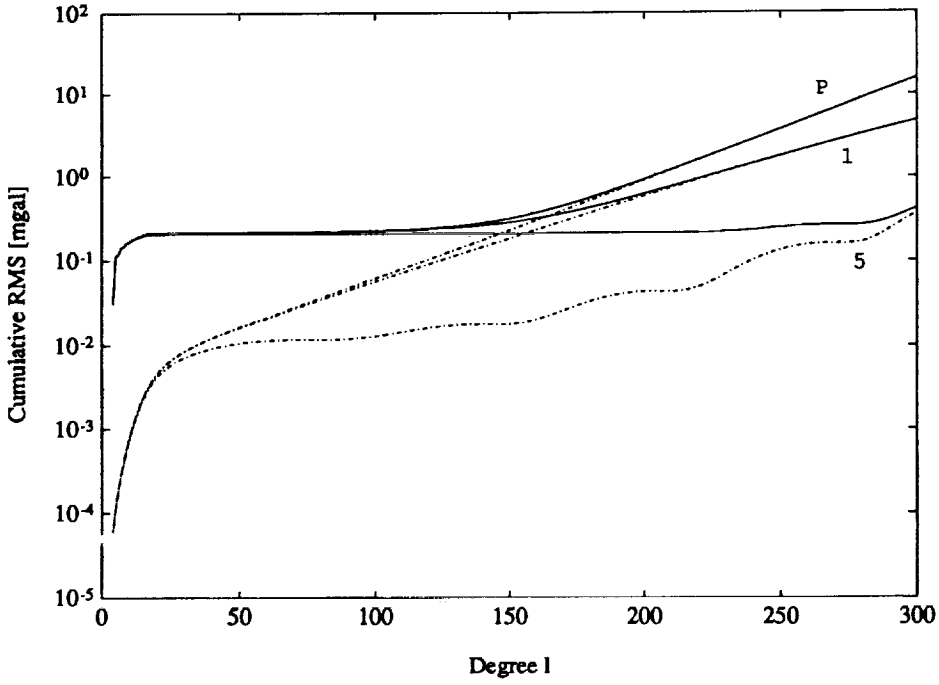

Figure 3.11: The cumulative point, 1° and 5° mean $\delta_l(\Delta g)$ values for the combined GPS and gradiometer solutions. Dashed: with GPS, solid: without GPS. These values are derived from cases 1 and 3 shown in figure 3.9.

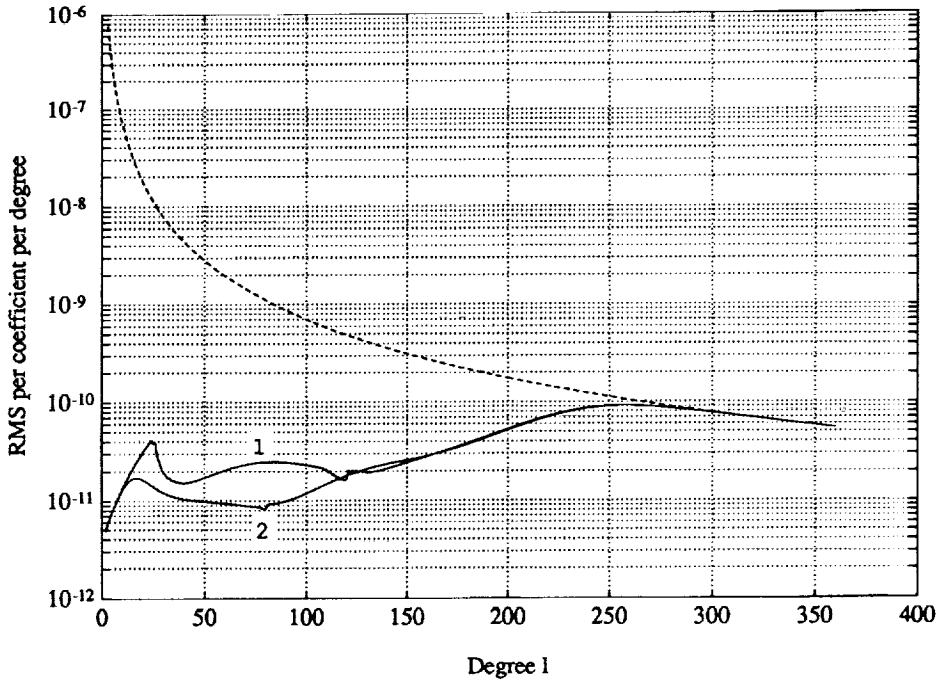

Figure 3.12: The mean r.m.s. per coefficient per degree for the combined GPS and gradiometer solutions pursuing a hybrid norm approach. Curve 1: Gradiometer: $27 < \beta < \infty$, L=360; GPS: $0 < \beta < \infty$, L=120. Curve 2: Gradiometer: $4 < \beta < \infty$, $\beta_{min} = 27$ ($1/\beta$ below β_{min}), L=300; GPS: $0 < \beta < \infty$, L=80. In both cases we assumed a mission duration of 6 months, 4 s sampling time and 0.01 E instrumental noise for the gradiometer, while measuring T_{uu}, T_{uw} and T_{ww}. For the GPS receiver we assumed a sampling time of 1 s and 3 cm noise in the position estimates.

Chapter 4

Conclusions and Recommendations

The discussion in Chapter 2 has shown that a gradiometer mission at 200 km with no drag compensation poses several constraints on the design of the instrument, the satellite, the choice of the nominal orbit and the accuracy of attitude restitution. In an ideal case, the orbit of a gradiometer satellite should be as low as possible, e.g. 160-200 km, near circular and allowing a global coverage of the gravity field demanding that $I = 90°$. However in practice sun-synchronous orbits are chosen [$I = 96.33°$ at 200 km] to provide an efficient means of power production using solar arrays.

A 2-axis 0.01 E/$\sqrt{\text{Hz}}$, gradiometer has been proposed for launch near the end of this decade [1996-1998] on a satellite called Aristoteles. The mission objectives are to measure the global gravity field in order to obtain geoid heights and gravity anomalies to within 10 cm and 5 mgal respectively.

A treatment of the error sources reveals that orbit errors of several meters appear to be no real problem for a 0.01 E/$\sqrt{\text{Hz}}$ gradiometer. The errors caused in the gravity gradients are mostly in the low frequency band and can be eliminated by filtering the signal below 4 cpr for a 10^{-2} E instrument, whereas filtering below 25 cpr is needed for a 10^{-4} E instrument.

A static approach to the attitude problem for Aristoteles shows that pitch and yaw rotational velocities need to be known to within 5×10^{-9} and 10^{-8} rad/s respectively which poses a severe constraint on the attitude restitution of the instrument, cf (ESA,1989). According to this report modern gyroscopes obtain an accuracy of 10^{-7} rad/s inside the measurement bandwidth which is unfortunately still a factor 10 to 20 too large for an adequate attitude reconstruction.

A dynamic approach of the attitude problem shows that rotational velocities, and thereby gradiometer signal errors, are decaying at a rate inversely proportional to the frequency of the disturbing torque function. A simulation of the dynamic

attitude problem discussed in Appendix A shows that the atmospheric torques on the non-drag free satellite are probably too high for a 0.01 E gradiometer.

This means that the static approach already answered the question: highly accurate gyroscopes possibly combined with star trackers are required for attitude restitution. We conclude that additional studies are required to determine whether this is feasible by application of modern processing techniques and/or technology resulting in an acceptable solution within the budgetary constraints.

Additionally the problem of scale, coupling and non-linearity errors in the accelerometers is discussed which allows non-conservative forces such as atmospheric drag to degrade the instrument performance cf Touboul et al. (1990). They conclude that the velocity vector of the spacecraft must be as perpendicular as possible to the gradiometer plane. This configuration might require a so-called yaw-steering mode of Aristoteles which compensates for a cross-track winds near the poles, see also (ESA,1989).

In Chapter 3 the results of an analytical error analysis of gravity field parameters are discussed assuming various scenarios proposed for Aristoteles [gradiometer and GPS receiver], Topex [GPS] and GP-B [GPS]. This analytical technique requires a nominal circular orbit having a repeat ratio compatible with the highest degree and order of the gravity field. Observation equations for both the GPS and the gradiometer part are derived in terms of lumped coefficient equations. The error analysis itself is based on variances being the elements of the inverted least squares [or hybrid norm] normal matrix which are converted to cumulative mean errors for gravity anomalies and geoid heights.

The error analysis shows that limited bandwidths of the gradiometer of Aristoteles seriously affect the outcome of an error analysis. Especially the lower degree and orders of the gravity solution deteriorate rapidly when restricting the lower end of the noise spectrum which is related to thermal noise in the gradiometer and e.g. atmospheric drag causing disturbing torques on the spacecraft. It was also recognized for both gradiometer and GPS observation equations that the choice of the inclination of the orbital plane plays an important role since the formal errors of potential coefficients tend to deteriorate when the inclination is several degrees off the polar inclination.

The most promising solutions for Aristoteles were obtained by combining GPS and gradiometer observations. It is shown that 1) GPS and gradiometer derived solutions are almost complementary, 2) that errors in recovered geoid heights are particulary determined by uncertainties in the lower degree and orders of the gravity field, 3) the original Aristoteles mission objectives [$\epsilon(\Delta g) < 5$ mgal and $\epsilon(N) < 10$ cm up to $\lambda = 100$ km] are hard to meet without the availability of GPS as a tracking facility and that 4) without the availability of GPS the objectives are easier met for gravity anomalies than geoid heights. A worst case drag simulation using gradiometer and GPS observation equations shows that the inclination problem [a

slightly non-polar orbit] and the bandwidth problem may be avoided by adding GPS observation equations to sufficient high degree and order of the geopotential model while pursuing a hybrid norm approach.

The results presented in this study should be interpreted in the sense of an error analysis rather than a final solution for the gradiometer/GPS problem. GPS data may be processed by numerical techniques as was demonstrated by Pavlis et al. (1989) for Topex. Gradiometer data could be processed by using the GPS gravity field solution simultaneously with the measured tensor components in a least squares collocation approach cf (Moritz,1980) to predict a grid of values on a sphere. An actual potential coefficient set, to represent the true nature of the short wavelength gravity information, could then be derived by numerical analysis methods using orthogonality properties of Legendre functions. This is very similar to the technique for deriving gravity field solutions from altimeter data and terrestial gravity anomalies cf (Rapp & Cruz,1986).

Bibliography

[1] Benz R., Faulks H. and Langemann M. (1988) *Aristoteles - An European approach for an Earth gravity field recovery mission*, in proc.: Chapman Conference on Progress in the Determination of the Earth's Gravity Field, Fort Lauderdale, Florida.

[2] Bettadpur S. (1990), *Personal communication*

[3] Betti B. and Sansò F. (1988) *The integrated approach to satellite geodesy*, Paper presented on the summer school in Assisi, Italy.

[4] Colombo O.L. (1986) *Notes on the Mapping of the Gravity Field Using Satellite Data*, Paper presented on the summer school in the mountains, Admont, Austria, 1986. Bundled lecture notes are available in the Springer Verlag series on Earth sciences ISBN 3-540-16809-5 or ISBN 0-387-16809-5.

[5] Colombo O.L. (1988) *High resolution Analysis of Satellite Gradiometry*, in proc.: Chapman Conference on Progress in the Determination of the Earth's Gravity Field, Fort Lauderdale, Florida.

[6] ESA (1989) *Aristoteles phase-A study*

[7] Hajela D.P. (1978) *Improved procedures for the recovery of* 5° *mean gravity anomalies from ATS-6/GEOS-3 satellite to satellite range-rate observations using least squares collocation*, Rep. AFGL TR-78-0260, Air Force Geophysical Lab., Hanscom Air Force Base Mass.

[8] Hearn A.C. (1985) *Reduce User's Manual*, Version 3.2, publ. no. CP78, Rev. 4/85, The Rand corporation, Santa Monica, CA 90406.

[9] Heikanen W.A. and Moritz H. (1979) *Physical Geodesy*, Original edition published in 1967 by W.H. Freeman and Company San Francisco. Now available from: Institute of Physical Geodesy Steyergasse 17, A-8010 Graz, Austria.

[10] Kaplan M.H. (1976) *Modern Spacecraft Dynamics and Control*, John Wiley and Sons, New York ISBN 0-471-45703-5.

[11] Katsambalos K.E. *The Effect of the Smoothing Operator on Potential Coefficient Determinations*, The Ohio State University, Report No. 287. (1979)

[12] Kaula W.M. (1966a) *Theory of Satellite Geodesy*, Blaisdell Publishing Co.

[13] Kaula W.M. (1966b) *Tests of Satellite Determinations of the Gravity Field Against Gravimetry and Their Combination*, Publication No. 509, Institute of Geophysics and Planetary Physics, University of California, 1966.

[14] Keating T., Taylor P., Kahn W. and Lerch F. (1986) *Geopotential Research Mission, science, engineering and program summary*, NASA/GSFC Technical Memorandum 86240.

[15] Koop R., Schrama E., Rummel R. & Gelderen M. van (1989) *Gravity Field Recovery Performance*, Project: Aristoteles Add-on study part1, W.P. NO. 2420/1, Delft University of Technology.

[16] Marsh J.G., Lerch F.J., Putney B.H., Christodoulidis D.C., Felsentreger T.L., Sanchez B.V., Smith D.E., Klosko S.M., Martin T.V., Pavlis E.C., Robbins J.W., Williamson R.G., Colombo O.L., Chandler N.L., Rachlin K.E., Patel G.B., Bhati S. and Chinn D.S. (1986) *An Improved Model of the Earth's Gravitational Field GEM-T1*, Goddard Space Flight Center, NASA technical memorandum 4019.

[17] Marsh J.G., Lerch F.J., Putney B.H., Felsentreger T.L., Sanchez B.V., Klosko S.M., Patel G.B., Robbins J.W., Williamson R.G., Engelis T.E., Eddy W.F., O.L., Chandler N.L., Chinn D.S., Kapoor S., Rachlin K.E., Braatz L.E. and Pavlis E.C. (1989) *The GEM-T2 Gravitational model*, Goddard Space Flight Center, NASA Technical memorandum 100746.

[18] Martin T.V., Oh I.H., Eddy W.F., Kogut J.A. (1976) em Geodyn System Description, Vol 1, Report NASA, Goddard Space Flight Center.

[19] Morgan S.H. and Paik H.J. (editors) (1988) *Superconducting Gravity Gradiometer Mission*, Vol. II, Study team technical report, NASA Technical Memorandum 4091.

[20] Moritz H. (1980) *Advanced Physical Geodesy*, Herbert Wichmann Verlag ISBN 3-87907-106-3, Abacus Press ISBN 0-85626-195-5.

[21] Pavlis E.C. and Smith D.E. (1989) *Expected Gravity Field Improvement from GPS Tracking of TOPEX*, Presented at the fall meeting of the American Geophysical Union, San Francisco, CA.

[22] Rapp R.H. and Cruz J. (1986) *Development and Comparison of High Degree Spherical Harmonic Models of the Earth's Gravity Field*, paper presented at the symposium "Definition of the Geoid", Florence, Italy.

[23] Rapp R.H. (1988) *Signals and accuracies to be Expected from a Gravity Gradiometer Mission*, Ohio State University, Dept. of Geodetic Science and Surveying, Columbus, Ohio.

[24] Ridgway J.R. (1990), *Personal Communication*

[25] Rummel R. and Colombo O.L. (1985) *Gravity Field Determination from Satellite Gradiometry*, Bulletin Geodesique, 59,3,233-246.

[26] Rummel R. (1986) *Satellite Gradiometry*, presented on the summer school in the mountains, Admont, Austria, 1986. Bundled lecture notes are available in the Springer Verlag series on Earth sciences ISBN 3-540-16809-5 or ISBN 0-387-16809-5.

[27] Schrama E.J.O. (1989a) *The role of orbit errors in processing of satellite altimeter data*, Netherlands Geodetic Commission, Delft, No 33.

[28] Schrama E.J.O. (1989b) Technical Memorandum to ESA/Estec, Dornier, Onera and Matra/Espace concerning the predictability of T_{xz} by means of existing gravity models, Dep. of Geodesy, Delft University of Technology.

[29] Smith D.E., Lerch F.J., Colombo O.L., Everitt C.W.F. (1988) *Gravity Field Information from Gravity Probe-B*, in proc.: Chapman Conference on Progress in the Determination of the Earth's Gravity Field, Fort Lauderdale, Florida.

[30] Touboul P., Bernard A., Barlier F. and Berger C. (1990) *Air drag effect on gradiometer measurements*, submitted to manuscripta geodaetica.

[31] Vaníček P. and Krakiwsky E. (1984) *Geodesy, The Concepts*, second edition Elsevier Science Publishers ISBN 0-444-87775-4 and ISBN 0-444-87777-0 (pbk.)

[32] Vonbun F.O., Kahn W.D., Wells W.T. and Conrad T.D. (1980) *Determination of* $5° \times 5°$ *gravity anomalies using satellite-to-satellite tracking between ATS-6 and Apollo*, Geophys. J.R. Astron. Soc., 61, 645-657.

[33] Wolff M. (1969) *Direct measurements of the Earth's gravitational potential using a satellite pair*, Journal of Geophysical Research, 74, p. 5295-5300.

Appendix A

Attitude error simulation.

In this Appendix the dynamic behavior of attitude errors is discussed. The equations used in this simulation are (2.20), the non-resonant particular solution of the linearized Newton-Euler equations including gravitational torques, and eq. (2.14) relating these rotational velocity errors to gravity gradient errors.

Moments of inertia

At the time of writing moments of inertia are not published for Aristoteles. In order to avoid the laborious task of computing precise moments of inertia we assumed that the principle axes of inertia could be derived from a homogenous cylinder representing the satellite's bus, a plate representing the solar arrays and a thin rod pointing forward for the magnetometer boom. Additionally we assumed various dimensions and weights of these elements; the total configuration is shown in figure A.1. The values found for the moments of inertia are $I_1 = 284.3$ [radial anti-Earth pointing], $I_2 = 476.3$ and $I_3 = 303.1\ kg/m^2$.

The algorithm

The algorithm assumes a so-called torque noise level variable $[TNL]$ which defines R_i in eqns. (2.19) as $R_i = TNL/I_i$. This allows to evaluate the derivatives of θ_i with respect to time in eq. (2.20) for a given β symbolizing the frequency in cpr in the torque noise spectrum. The resulting variables $\dot{\theta}_1$ and $\dot{\theta}_3$ are then substituted in (2.14) resulting in sine-cosine expressions for $\Delta\Gamma_{11}$ and $\Delta\Gamma_{13}$ [namely $a\cos(\beta n_0 t) + b\sin(\beta n_0 t)$]. The amplitudes $c = (a^2 + b^2)^{1/2}$ are an indication of the errors in T_{uu} and T_{uw} showing the expected $1/\beta$ behavior. Figure A.2 represents the values of TNL on the y-axis and β on the x-axis for $c = 0.01$ and $c = 0.0001$ E.

This simulation shows that the lower end of the effective frequency bandwidth of T_{uu} [solid line] and T_{uw} [dashed line] is determined by the noise level of the torques acting on the satellite. The tensor component T_{uw} shows a minimal frequency ap-

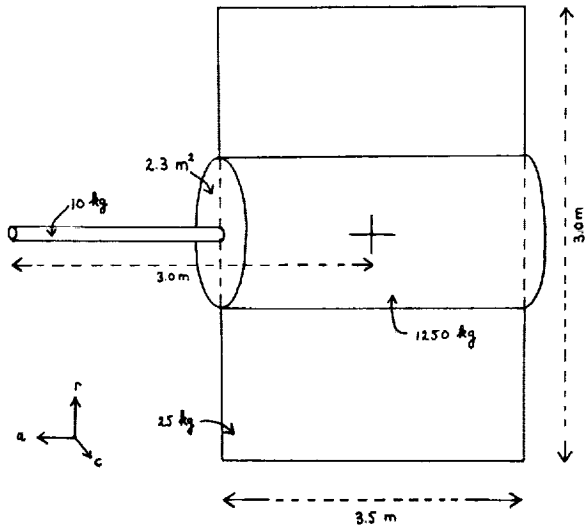

Figure A.1: Elements dimensions and weights used for the estimation of moments of inertia of Aristoteles.

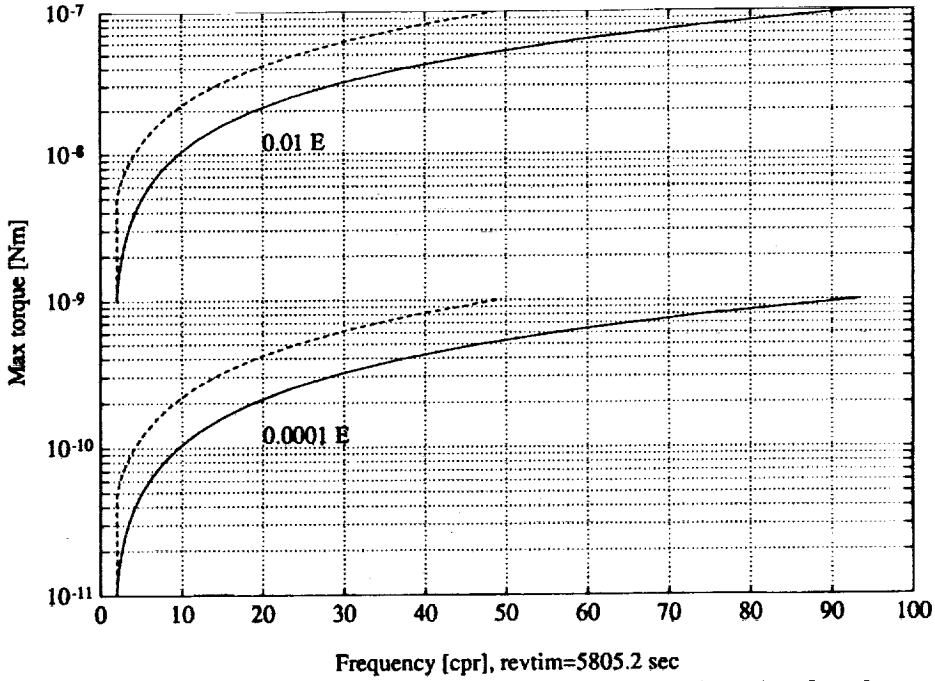

Figure A.2: Maximal allowed torques vs. frequency assuming simulated moments of inertia of Aristoteles.

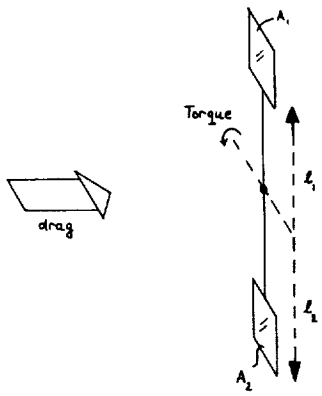

Figure A.3: Symmetry, torques, atmospheric drag

proximately twice as low as T_{uu}. T_{ww} is not considered in the simulation since it is the only tensor component in this configuration that is not modulated by n_0. [see eq. (2.14)] Resonance problems are not plotted in figure A.2, the results are shown above 2 cpr. All resonant frequencies occur at 1.08 and 0.29 cpr for θ_1 and θ_2 , $\beta = 1.38$ cpr for θ_3.

Maximal allowed torque noise level

In a non-drag free environment the noise level of the torques itself is mainly determined by non-conservative forces such as drag acting on the bus and appendages of the spacecraft. It is also determined by symmetry of the projected area normal to the velocity vector of the spacecraft and the spectral behavior of drag variations.

An example of symmetry of the projected area, torques and atmospheric drag acting on the satellite is displayed in figure A.3. In this example the torque effect due to drag equals to:

$$T = \frac{1}{2}\rho v^2 C_d (l_1 A_1 - l_2 A_2). \tag{A.1}$$

For a maximal torque noise level of 3×10^{-8} Nm and a 0.01 E gradiometer the results displayed in figure A.2 allow the lower end of the bandwidths of T_{uu} and T_{uw} to start at respectively 29.58 and 14.80 cpr. At 200 km height $\rho \approx 3 \times 10^{-10}\ kg/m^3$ and $v \approx 7784.3\ m/s^2$ whereas $C_d = 3$ for Aristoteles, so that in figure A.3:

$$3 \times 10^{-8} = \frac{1}{2}\rho v^2 C_d \Delta (l_1 A_1 - l_2 A_2)$$

requiring that

$$\Delta (l_1 A_1 - l_2 A_2) \leq 10^{-6} \tag{A.2}$$

which is a very stringent requirement for symmetry of projected surfaces and their distances to the principal axes, even if a so-called yaw steering mode is pursued. However Touboul et al. (1990) report that the expected drag fluctuations, having wavelengths shorter than 200 s, may contain only 5% of the power of the total drag force. Even this assumption might be too stringent for condition (A.2) since it would mean that the uncertainties in l_1 and l_2 have to remain below 1 to 10 μm which is unlikely taking into account phenomena such as thermal expansion due to heating and cooling of the spacecraft. We conclude that attitude restitution must be provided by measurements from gyroscopes and star trackers once the gradiometer is subject to atmospheric drag. In case a drag free or a shielded gradiometer is considered the torque noise level is reduced substantially thereby increasing the bandwidth of the gradiometer and relaxing the need for a highly accurate attitude reconstruction.

Appendix B

Expressions for gravity gradients

In this Appendix the following coordinate systems and indices are used:

- $u_i = \{u, v, w\}$: the gradiometer instrument system (u: radial, v: along track and w: cross track),
- $r_a = \{r, \omega_o, \omega_e\}$ and $r_a = \{r, \omega_o, I\}$: subsets of the total set of orbital parameters $\{r, \omega_o, \omega_e, I\}$,
- $x_p = \{x, y, z\}$: the geocentric system.

The following relation exists:

$$\overline{x} = R_3(-\omega_e)R_1(-I)R_3(-\omega_o)\begin{bmatrix} \alpha \\ \beta \\ \gamma \end{bmatrix} \tag{B.1}$$

where α, β and γ are linearized as $\alpha = r + u$, $\beta = v$ and $\gamma = w$. Here the potential function T is defined in the r_a system, see eqns. (3.1) through (3.4), whereas derivatives of T are needed in the gradiometer instrument frame u_i:

$$\frac{\partial T}{\partial u_i} = \frac{\partial T}{\partial r_a}\frac{\partial r_a}{\partial u_i} \tag{B.2}$$

The tensor of second order derivatives in the u_i system is obtained by differentiating once again with respect to u_j:

$$\frac{\partial^2 T}{\partial u_i \partial u_j} = \frac{\partial^2 T}{\partial r_a \partial r_b}\frac{\partial r_a}{\partial u_i}\frac{\partial r_b}{\partial u_j} + \frac{\partial T}{\partial r_a}\frac{\partial^2 r_a}{\partial u_i \partial u_j}. \tag{B.3}$$

To evaluate (B.3) the first and second order derivatives of the r_a to the u_i system are needed. These expressions are derived in the following way:

$$\frac{\partial r_a}{\partial u_i} = \left[\frac{\partial x_p}{\partial r_a}\right]^{-1} \frac{\partial x_p}{\partial u_i} \tag{B.4}$$

$$\frac{\partial^2 r_a}{\partial u_i \partial u_j} = \left[\frac{\partial x_p}{\partial r_a}\right]^{-1} \left\{ \frac{\partial^2 x_p}{\partial u_i \partial u_j} - \frac{\partial^2 x_p}{\partial r_a \partial r_b} \frac{\partial r_a}{\partial u_i} \frac{\partial r_b}{\partial u_j} \right\} \tag{B.5}$$

where the derivatives of x_p to r_a and of x_p to u_i are computed from eq.(B.1). The formula manipulation program REDUCE, developed by Hearn et al. (1985), is used to develop the full tensor of second order derivatives of the form of (B.3). [the evaluations of (B.3), (B.4) and (B.5) are rather lengthy] The expressions found which are independent of the choice of r_a are: [notation: $\frac{\partial T}{\partial r} = T_r$, $\frac{\partial T}{\partial \omega_o} = T_o$, $\frac{\partial T}{\partial \omega_e} = T_e$, etc.]

$$T_{uu} = T_{rr} \tag{B.6}$$

$$T_{vv} = \frac{1}{r^2} T_{oo} + \frac{1}{r} T_r \tag{B.7}$$

$$T_{ww} = -T_{rr} - \frac{1}{r^2} T_{oo} - \frac{1}{r} T_r \tag{B.8}$$

$$T_{uv} = \frac{1}{r} T_{ro} - \frac{1}{r^2} T_o \tag{B.9}$$

The terms T_{uw} and T_{vw} depend on the choice of r_a:

$$T_{uw} = \frac{1}{r \sin \omega_o} \{ T_{rI} - \frac{1}{r} T_I \} \tag{B.10}$$

$$T_{uw} = \frac{1}{r \cos \omega_o \sin I} \{ (\frac{1}{r} T_e - T_{re}) + \cos I (-\frac{1}{r} T_o + T_{ro}) \} \tag{B.11}$$

and

$$T_{vw} = \frac{1}{r^2 \sin \omega_o} \{ T_{oI} - \frac{\cos \omega_o}{\sin \omega_o} T_I \} \tag{B.12}$$

$$T_{vw} = \frac{1}{r^2 \cos^2 \omega_o \sin I} \times \{ \cos \omega_o (-T_{oe} + T_{oo} \cos I) + \sin \omega_o (-T_e + T_o \cos I) \} \tag{B.13}$$

Multiplication of (B.10) times $\sin^2 \omega_o$ and adding (B.11) times $\cos^2 \omega_o$ results in:

$$T_{uw} = \{ \sin^{-1} I \{ -\frac{1}{r} T_{re} + \frac{1}{r^2} T_e \} + \frac{\cos I}{\sin I} \{ \frac{1}{r} T_{ro} - \frac{1}{r^2} T_o \} \} \cos \omega_o + \{ \frac{1}{r} T_{rI} - \frac{1}{r^2} T_I \} \sin \omega_o \tag{B.14}$$

In a similar way (B.12) times $\sin^2\omega_o$ added to (B.13) times $\cos^2\omega_o$ results in:

$$\begin{aligned} T_{vw} &= \{\frac{-1}{r^2\sin I}T_{eo} + \frac{\cos I}{r^2\sin I}T_{oo} - \frac{1}{r^2}T_I\}\cos\omega_o + \\ &\quad \{\frac{-1}{r^2\sin I}T_e + \frac{\cos I}{r^2\sin I}T_o + \frac{1}{r^2}T_{oI}\}\sin\omega_o \end{aligned} \tag{B.15}$$

While using expressions similar to (B.10) through (B.13) Betti and Sansò (1988) introduced so-called $\overline{F}^*_{lmp}$ functions which are modifications of the original inclination functions. These modified functions are needed to avoid singularities at $\omega_o = k\frac{\pi}{2}$ in eqns. (B.10) to (B.13). Moreover it is desirable to obtain expressions where all time dependent effects are contained in the derivatives of T in the r_a system [or T^* in Betti and Sanso's approach].

Here we use expressions (B.14) and (B.15) which merely require to multiply a Fourier series by sine and cosine terms thereby avoiding to introduce modified inclination functions which would require to change the existing algorithm to compute inclination functions and their derivatives, cf (Schrama,1989a). A multiplication of a Fourier series once by a sine and once by a cosine term similar to the structure of eqns. (B.14) and (B.15) is not very complicated, one can show that:

$$\begin{aligned} \sum_{k=-L}^{L}\sum_{m=0}^{L} & (A^c_{km}\cos\psi_{km} + B^c_{km}\sin\psi_{km})\cos\psi_{km} + \\ & (A^s_{km}\cos\psi_{km} + B^s_{km}\sin\psi_{km})\sin\psi_{km} \end{aligned} \tag{B.16}$$

equals to

$$\sum_{k=-L-1}^{L+1}\sum_{m=0}^{L} A_{km}\cos\omega_o + B_{km}\sin\omega_o \tag{B.17}$$

where

$$A_{km} = \frac{1}{2}(+A^c_{k-1,m} + A^c_{k+1,m}) + \frac{1}{2}(-B^s_{k-1,m} + B^s_{k+1,m}) \tag{B.18}$$

$$B_{km} = \frac{1}{2}(+A^s_{k-1,m} - A^s_{k+1,m}) + \frac{1}{2}(+B^c_{k-1,m} + B^c_{k+1,m}) \tag{B.19}$$

and

$$A^{c,s}_{km} = B^{c,s}_{km} = 0 \quad \text{for} \quad |k| > L. \tag{B.20}$$

NASA
National Aeronautics and Space Administration

Report Documentation Page

1. Report No.	2. Government Accession No.	3. Recipient's Catalog No.
NASA TM-100769		

4. Title and Subtitle

Gravity Field Error Analysis:
Applications of GPS Receivers and Gradiometers
on Low Orbiting Platforms

5. Report Date

November 1990

6. Performing Organization Code

Code 626

7. Author(s)

E. Schrama

8. Performing Organization Report No.

91E00216

10. Work Unit No.

9. Performing Organization Name and Address

Space Geodesy Branch
Goddard Space Flight Center
Greenbelt, MD 20771

11. Contract or Grant No.

13. Type of Report and Period Covered

Technical Memorandum

12. Sponsoring Agency Name and Address

National Aeronautics and Space Administration
Washington, DC 20546-0001

14. Sponsoring Agency Code

15. Supplementary Notes

16. Abstract

The concept of a GPS receiver as a tracking facility and a gradiometer as a separate instrument on a low orbiting platform offers a unique tool to map the Earth's gravitational field with unprecedented accuracies. The former technique allows determination of the spacecraft's ephemeris at any epoch to within 3 to 10 cm, the latter permits the measurement of the tensor of second order derivatives of the gravity field to within 0.01 to 0.0001 Eötvös units depending on the type of gradiometer. The first part of this report describes a variety of error sources in gradiometry where emphasis is placed on the rotational problem pursuing as well a static as a dynamic approach. In the second part, an analytical technique is described and applied for an error analysis of gravity field parameters from gradiometer and GPS observation types. Results are discussed for various configurations proposed on Topex/Poseidon, Gravity Probe-B and Aristoteles, indicating that "GPS only" solutions may be computed up to degree and order 35,55 and 85 respectively, whereas a combined GPS/gradiometer experiment on Aristoteles may result in an acceptable solution up to degree and order 240.

17. Key Words (Suggested by Author(s))	18. Distribution Statement
Gravity Fields, Gradiometry, Geodesy, and GPS	Unclassified - Unlimited Subject Category 42

19. Security Classif. (of this report)	20. Security Classif. (of this page)	21. No. of pages	22. Price
Unclassified	Unclassified	56	

NASA FORM 1626 OCT 86

PREPARATION OF THE REPORT DOCUMENTATION PAGE

The last page of a report facing the third cover is the Report Documentation Page, RDP. Information presented on this page is used in announcing and cataloging reports as well as preparing the cover and title page. Thus it is important that the information be correct. Instructions for filling in each block of the form are as follows:

Block 1. Report No. NASA report series number, if preassigned.

Block 2. Government Accession No. Leave blank.

Block 3. Recipient's Catalog No. Reserved for use by each report recipient.

Block 4. Title and Subtitle. Typed in caps and lower case with dash or period separating subtitle from title.

Block 5. Report Date. Approximate month and year the report will be published.

Block 6. Performing Organization Code. Leave blank.

Block 7. Author(s). Provide full names exactly as they are to appear on the title page. If applicable, the word editor should follow a name.

Block 8. Performing Organization Report No. NASA installation report control number and, if desired, the non-NASA performing organization report control number.

Block 9. Performing Organization Name and Address. Provide affiliation (NASA program office, NASA installation, or contractor name) of authors.

Block 10. Work Unit No. Provide Research and Technology Objectives and Plans (RTOP) number.

Block 11. Contract or Grant No. Provide when applicable.

Block 12. Sponsoring Agency Name and Address. National Aeronautics and Space Administration, Washington, D.C. 20546-0001. If contractor report, add NASA installation or HQ program office.

Block 13. Type of Report and Period Covered. NASA formal report series; for Contractor Report also list type (interim, final) and period covered when applicable.

Block 14. Sponsoring Agency Code. Leave blank.

Block 15. Supplementary Notes. Information not included elsewhere: affiliation of authors if additional space is required for block 9, notice of work sponsored by another agency, monitor of contract, information about supplements (film, data tapes, etc.), meeting site and date for presented papers, journal to which an article has been submitted, note of a report made from a thesis, appendix by author other than shown in block 7.

Block 16. Abstract. The abstract should be informative rather than descriptive and should state the objectives of the investigation, the methods employed (e.g., simulation, experiment, or remote sensing), the results obtained, and the conclusions reached.

Block 17. Key Words. Identifying words or phrases to be used in cataloging the report.

Block 18. Distribution Statement. Indicate whether report is available to public or not. If not to be controlled, use "Unclassified-Unlimited." If controlled availability is required, list the category approved on the Document Availability Authorization Form (see NHB 2200.2, Form FF427). Also specify subject category (see "Table of Contents" in a current issue of STAR), in which report is to be distributed.

Block 19. Security Classification (of this report). Self-explanatory.

Block 20. Security Classification (of this page). Self-explanatory.

Block 21. No. of Pages. Count front matter pages beginning with iii, text pages including internal blank pages, and the RDP, but not the title page or the back of the title page.

Block 22. Price Code. If block 18 shows "Unclassified-Unlimited," provide the NTIS price code (see "NTIS Price Schedules" in a current issue of STAR) and at the bottom of the form add either "For sale by the National Technical Information Service, Springfield, VA 22161-2171" or "For sale by the Superintendent of Documents, U.S. Government Printing Office, Washington, DC 20402-0001," whichever is appropriate.

U.S. GOVERNMENT PRINTING OFFICE 1980 O—944-511